

# FAST DIVERSITY-PRESERVING REWARD FINETUNING OF DIFFUSION MODELS VIA NABLA-GFLOWNETS

**Anonymous authors**

Paper under double-blind review

## ABSTRACT

While one commonly trains large diffusion models by collecting datasets on target downstream tasks, it is often desired to finetune pretrained diffusion models on some reward functions that are either designed by experts or learned from small-scale datasets. Existing methods for finetuning diffusion models typically suffer either 1) lack of diversity in generated samples, or 2) costly finetuning and slow convergence. Inspired by recent successes in generative flow networks (GFlowNets), a class of probabilistic models that sample with the unnormalized density of a reward function, we propose a novel GFlowNet method dubbed Nabla-GFlowNet (abbreviated as  $\nabla$ -GFlowNet), together with an objective called  $\nabla$ -DB, plus its variant *residual*  $\nabla$ -DB for finetuning pretrained diffusion models. These objectives leverage the rich signal in reward gradients for diversity-aware finetuning. We empirically show that our proposed *residual*  $\nabla$ -DB achieves fast yet diversity- & prior-preserving finetuning of StableDiffusion, a large-scale text-conditioned image diffusion model, on different realistic reward functions.

## 1 INTRODUCTION

Diffusion models [14, 50, 41] are a powerful class of generative models that model highly complex data distributions as the results of a sequence of multi-scale denoising steps. They prove capable of generating with high-fidelity a wide range of entities, including but not limited to images [41, 9], videos [15], 3D objects [69, 38, 28, 29], molecules [61, 16], languages [43]. State-of-the-arts diffusion models for downstream applications are typically large in network size and demand a significant amount of data to train.

It is however often desirable that one finetunes a pretrained diffusion models with a given reward function — either from some learned reward function in the scenario of reinforcement learning from human feedback (RLHF) [6, 34] or from some expert design [47, 33]. While existing methods achieve fast convergence of reward maximization [60, 7], typically through reinforcement learning, many of these methods are either mode-seeking and fail in generating diverse samples or too expensive to use in large-scale settings.

Inspired by recent work in generative flow networks (GFlowNets), a class of probabilistic models that aim to sample from unnormalized density distributions, we propose a novel training objective, dubbed  $\nabla$ -DB, that leverages the rich information in reward gradients. The variant *residual*  $\nabla$ -DB, by leveraging the structure of diffusion models, allows us to perform fast, diversity preserving and prior-preserving amortized finetuning with rather long sampling sequences of diffusion models.

We summarize our contributions below:

- We propose  $\nabla$ -DB, a novel objective for GFlowNets that leverages the rich information in reward gradients.
- For the purpose of finetuning with a pretrained prior, we propose a variant called *residual*  $\nabla$ -DB that leverages the properties of diffusion models for efficient finetuning.
- We empirically show that with the propose *residual*  $\nabla$ -DB objective, we may achieve diversity-preserving yet fast finetuning of diffusion models.

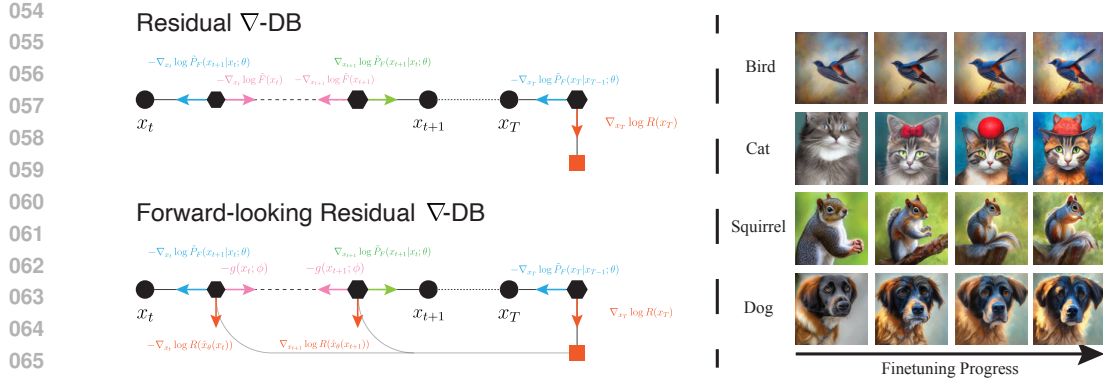


Figure 1: Left: Illustration of the proposed *residual*  $\nabla$ -DB objective, along with its forward-looking variant. All “forces” (from the finetuned diffusion model, the pretrained model, the reward gradient and the learned flow function) on each hexagon should add to zero. Right: Generated image from a model finetuned with the proposed *residual*  $\nabla$ -DB on Aesthetic Score reward. The text prompt for each row is shown on the left. The leftmost figure is the image generated by the pretrained model while the rightmost one is from the model finetuned for 200 iterations.

## 2 PRELIMINARIES

### 2.1 DIFFUSION MODELS AND RL-BASED FINETUNING

Diffusion models [14, 48, 50] are a class of hierarchical latent models that model the generation process as a sequence of denoising steps. Different from the convention in diffusion model literature, for convenience we adopt in this paper the reverse time of arrow where  $x_T$  means samples from the data distribution and the sampling process starts from  $t = 0$ . Under this convention, the probability of the generated samples is:

$$P_F(x_T) = \int_{x_{0:T-1}} P_0(x_0) \prod P_F(x_t|x_{t-1}) dx_{0:T-1}. \quad (1)$$

Here  $P_0(x_0)$  is a fixed initial distribution,  $P_F(x_T)$  is the likelihood of the model generating data  $x_T$ , and the noisy states  $x_t$  in the intermediate time steps are constructed by a pre-defined noising process, and the *forward policy*  $P_F(x_t|x_{t-1})$  is the denoising step of the diffusion model<sup>1</sup>. Take DDPM [14] as an example: the corresponding noising process is  $q(x_{t-1}|x_t) = \mathcal{N}(\sqrt{\alpha_{t-1}/\alpha_t}x_t, \sqrt{1 - \alpha_{t-1}/\alpha_t}I)$ , which induces  $q(x_t|x_T) = \mathcal{N}(\sqrt{\alpha_{T-t}}x_T, \sqrt{1 - \alpha_{T-t}}I)$ , where  $\{\alpha_t\}_t$  is a noise schedule set. With this noising process defined, the training loss is:

$$\mathbb{E}_{t \sim \text{Uniform}(\{1, \dots, T\}), \epsilon \sim \mathcal{N}(0, I), x_T \sim \mathcal{D}} w(t) \left\| x_\theta(\sqrt{\alpha_{T-t}}x_T + \sqrt{1 - \alpha_{T-t}}\epsilon, t) - x_T \right\|^2, \quad (2)$$

where  $\mathcal{D}$  is a dataset,  $w(t)$  is a certain schedule weighting function, and  $x_\theta(x_t, t)$  is a data prediction model that predict the clean data  $x_T$  given a noisy data  $x_t$  at time step  $t$ .

The sequential sampling process of diffusion models is Markovian and one could construct an Markov decision process (MDP) to describe its denoising process. We refer to Black et al. [5], Zhang et al. [68] for details of the MDP specification. Given such an MDP defined, one may fine-tune diffusion models with techniques like DDPO [5] by collecting on-policy sample trajectories  $\{(x_1, \dots, x_T)\}$  and optimize the forward (denoising) policy with a given terminal reward  $R(x_T)$ .

### 2.2 GENERATIVE FLOW NETWORKS (GFLOWNETS)

GFlowNets [4, 2] are a class of probabilistic methods to train a sampling policy  $P_F(s'|s)$ , where the generation process starts from some initial state  $s_0$ , makes a series of stochastic transitions ( $s \rightarrow s'$ ) in a direct acyclic graph of states, and eventually reach a terminal state according to an unnormalized probability density, or reward. Similar to the role of noising process in diffusion

<sup>1</sup>The “forward” and “backward” directions in the GFlowNet literature are the opposite of those in the diffusion literature.

models, in GFlowNets a backward policy  $P_B(s|s')$  is defined (either fixed or learnable) to distribute the unnormalized density of the terminal target distribution back to its ancestor states. One may imagine that the forward policy  $P_F(s'|s)$  distributes density from all states  $s$  that lead to  $s'$  and similarly the backward policy  $P_B(s|s')$  distributes density from all states  $s'$  to an ancestor  $s$ . If  $P_F$  and  $P_B$  “matches” each other, one obtain on each state  $s$  an unnormalized density, called the flow function  $F(s)$ . One form of the matching condition states is the the detailed balance condition:

**Detailed Balance (DB).** A valid GFlowNet with a forward policy  $P_F(s'|s)$ , a backward policy  $P_B(s|s')$ , and a flow function  $F(s)$  satisfies the following DB condition for all transition ( $s \rightarrow s'$ )

$$P_F(s'|s)F(s) = P_B(s|s')F(s'). \quad (3)$$

Hence we have the following GFlowNet DB loss on the logarithm probability space:

$$L_{\text{DB}}(s, s') = \left( \log P_F(s'|s) + \log F(s) - \log P_B(s|s') - \log F(s') \right)^2 \quad (4)$$

with an extra terminal constraint  $F(s_f) = R(s_f)$  to incorporate target reward information.

In the context of time-indexed sampling processes such as diffusion models, the transition graph of states  $s \triangleq (x_t, t)$  is naturally acyclic, as it adheres to the arrow of time [63]. With slight abuse of terminology that we use  $x_t$  to represents the tuple  $(x_t, t)$  when necessary, for time-indexed settings the *forward policy* is  $P_F(x_{t+1}|x_t)$ , the *backward policy* is  $P_B(x_t|x_{t+1})$ , and the *flow function* is  $F(x_t)$ <sup>2</sup>. The corresponding DB condition is therefore

$$P_F(x_{t+1}|x_t)F(x_t) = P_B(x_t|x_{t+1})F(x_{t+1}). \quad (5)$$

To finetune a diffusion model with DB losses [68], one can simply set  $P_F(x_{t+1}|x_t)$  to be the sampling process and fix  $P_B(x_t|x_{t+1})$  to be the noising process used by the pretrained diffusion model. We refer to Zhang et al. [63], Lahlou et al. [23], Zhang et al. [67] for more detailed discussion about the theory of diffusion being a specification of GFlowNets.

### 3 METHOD

#### 3.1 $\nabla$ -DB: THE GRADIENT-INFORMED ALTERNATIVE TO DB

In our setting, we do not have access to any dataset of images, but are given an external positive-valued reward function  $R(\cdot)$  and we need to train a generative model to learn from it. While the GFlowNet-based algorithm can effectively achieve this and also encourages diversity, it only leverages the zeroth-order reward information and does not require any differentiability of the reward function. Yet, it is often beneficial to directly make use of the reward gradient as signal, since it brings higher dimensional information about the optimization landscape and thus enables more effective optimization. We are therefore motivated to develop  $\nabla$ -GFlowNet, a method that builds upon GFlowNet-based algorithms to take full advantage of the reward gradient signal. To achieve this, we take derivatives on the logarithms of both sides of the DB condition (logarithm of Equation 5) with respect to  $x_{t+1}$  and obtain a necessary condition, which we call the forward<sup>3</sup>  $\nabla$ -DB condition:

$$\nabla_{x_{t+1}} \log P_F(x_{t+1}|x_t) = \nabla_{x_{t+1}} \log P_B(x_t|x_{t+1}) + \nabla_{x_{t+1}} \log F(x_{t+1}), \quad (6)$$

and hence the corresponding forward  $\nabla$ -DB objective  $L_{\nabla\text{DB}}(x_t, x_{t+1})$  to be

$$\left\| \nabla_{x_{t+1}} \log P_F(x_{t+1}|x_t) - \nabla_{x_{t+1}} \log P_B(x_t|x_{t+1}) - \nabla_{x_{t+1}} \log F(x_{t+1}) \right\|^2, \quad (7)$$

with the terminal flow loss on the logarithm scale

$$L_{\nabla\text{DB-terminal}}(x_T) = \left\| \nabla_{x_T} \log F(x_T) - \beta \nabla_{x_T} \log R(x_T) \right\|^2, \quad (8)$$

where  $\beta$  is a temperature coefficient and serve as a hyperparameter in the experiments. Notice that, by taking derivatives on the logarithms, we obtain the score function  $\nabla_{x_{t+1}} \log P_F(x_{t+1}|x_t)$  of the

<sup>2</sup>We write  $F_t(x_t)$  as  $F(x_t)$  out of simplicity.

<sup>3</sup>Since the derivative is taken with respect to  $x_{t+1}$ .

finetuned diffusion model. Indeed, the  $\nabla$ -DB loss is closely related to a Fisher divergence, also known as Fisher information score [21] (see Appendix B.1).

Similarly, by taking the derivative of both sides in Equation 5 with respect to  $x_t$ , one obtains the reverse  $\nabla$ -DB objective:

$$L_{\nabla\text{-DB}}(x_t, x_{t+1}) = \left\| \nabla_{x_t} \log P_F(x_{t+1}|x_t) - \nabla_{x_t} \log P_B(x_t|x_{t+1}) + \nabla_{x_t} \log F(x_t) \right\|^2. \quad (9)$$

Such  $\nabla$ -GFlowNet objectives constitute a valid GFlowNet algorithm (see the proof in Section B.2):

**Proposition 1.** *If  $L_{\nabla\text{-DB}}(x_t, x_{t+1}) = L_{\nabla\text{-DB}}(x_t, x_{t+1}) = 0$  for any denoising transition  $(x_t, x_{t+1})$  over the state space and  $L_{\nabla\text{-DB-terminal}}(x_T) = 0$  for all terminal state  $x_T$ , then the resulting forward policy generate samples  $x_T$  with probability proportional to the reward function  $R(x_T)^\beta$ .*

**Remark 2.** The original detailed balance condition propagates information from the reward function to each state flow function in the sense of  $F(x_{t+1}) \rightarrow (F(x_t), P_F(x_{t+1}|x_t))$ , assuming the backward (noising) policy is fixed (*i.e.*, there is no learning component in the diffusion noising process). In our case, if we take a close look at Equation 7, we can see that  $L_{\nabla\text{-DB}}(x_t, x_{t+1})$  could propagate the information from  $F(x_{t+1})$  to the forward policy  $P_F(x_{t+1}|x_t)$  but not  $F(x_t)$ .

**Remark 3.** Compared to previous GFlowNet works which use a scalar-output network to parameterize the (log-) flow function, in  $\nabla$ -GFlowNet we can directly use a U-Net [42]-like architecture that (whose output and input shares the same number of dimension) to parameterize  $\nabla \log F(\cdot)$ , which potentially provides more modeling flexibility. Furthermore, it is possible to initialize  $\nabla \log F(\cdot)$  with layers from the pretrained model so that it can learn upon known semantic information.

### 3.2 RESIDUAL $\nabla$ -DB FOR REWARD FINETUNING OF PRETRAINED MODELS

With the  $\nabla$ -DB losses, one can already finetune a diffusion model to sample from the reward distribution  $R(x)$ . However, the finetuned model may eventually over-optimize the reward and thus forget the pretrained prior (*e.g.*, how natural images look like). Instead, similar to other amortized inference work [70, 56], we consider the following objective with an augmented reward:

$$P_F(x_T) \propto R(x_T)^\beta P_F^\#(x_T)^\eta, \quad (10)$$

where  $R(x)$  is the positive-valued reward function,  $\beta$  is the temperature coefficient,  $\eta$  is a parameter to control the strength of the prior,  $P_F^\#(x_T)$  is the marginal distribution of the pretrained model<sup>4</sup> and  $P_F(x_T)$  is the marginal distribution of the finetuned model (as defined in Equation 1).

Because both the finetuned and pretrained model share the same backward policy  $P_B$  (the noising process of the diffusion models), we can remove the  $P_B$  term and obtain the forward *residual*  $\nabla$ -DB condition by subtracting the forward  $\nabla$ -DB equation for the pretrained model from the that of the finetuned model:

$$\underbrace{\nabla_{x_{t+1}} \log P_F(x_{t+1}|x_t) - \eta \nabla_{x_{t+1}} \log P_F^\#(x_{t+1}|x_t)}_{\nabla_{x_{t+1}} \log \tilde{P}_F(x_{t+1}|x_t): \text{residual policy score function}} = \underbrace{\nabla_{x_{t+1}} \log F(x_{t+1}) - \nabla_{x_{t+1}} \log F^\#(x_{t+1}; \eta)}_{\nabla_{x_{t+1}} \log \tilde{F}(x_{t+1}): \text{residual flow score function}}. \quad (11)$$

With the two residual terms defined above, we obtain the forward *residual*  $\nabla$ -DB objective:

$$L_{\nabla\text{-DB-res}}(x_t, x_{t+1}) = \left\| \nabla_{x_{t+1}} \log \tilde{P}_F(x_{t+1}|x_t) - \nabla_{x_{t+1}} \log \tilde{F}(x_{t+1}) \right\|^2 \quad (12)$$

with the terminal flow loss in Equation 8. Similarly, we have the reverse *residual*  $\nabla$ -DB loss:

$$L_{\nabla\text{-DB-res}}(x_t, x_{t+1}) = \left\| \nabla_{x_t} \log \tilde{P}_F(x_{t+1}|x_t) + \nabla_{x_t} \log \tilde{F}(x_t) \right\|^2 \quad (13)$$

The terminal loss of the residual  $\nabla$ -DB method stays the same form as in Equation 8

$$L_{\nabla\text{-DB-terminal}}(x_T) = \left\| \nabla_{x_T} \log \tilde{F}(x_T) - \beta \nabla_{x_T} \log R(x_T) \right\|^2. \quad (14)$$

<sup>4</sup>We use the notation of # to indicate quantities of the pretrained model.



**Proposition 4.** If  $L_{\nabla\check{DB-res}}(x_t, x_{t+1}) = L_{\nabla\check{DB-res}}(x_t, x_{t+1}) = 0$  for any denoising transition  $(x_t, x_{t+1})$  over the state space and  $L_{\nabla DB-terminal}(x_T) = 0$  for all terminal state  $x_T$ , then the resulting forward policy generate samples  $x_T$  with probability proportional to  $R(x_T)^\beta P_F^\#(x_T)$ .

**Remark 5.** We point out that perform the same way of deriving Equation 11, i.e., subtraction between GFlowNet conditions from the finetuned and pretrained model, on the DB condition without gradient, we can obtain a *residual* DB condition  $\tilde{F}(x_t)P_F(x_{t+1}|x_t) = P_F^\#(x_{t+1}|x_t)\tilde{F}(x_{t+1})$ . Multiplying this condition across time and eliminate the term of intermediate  $\tilde{F}(x_t)$  will lead to the objective derived in the relative GFlowNet work [55] as shown in Section B.4, which is a prior paper that proposes to work on reward finetuning GFlowNets with a given pretrained model.

**Remark 6.** One may completely eliminate the need for any residual flow score function with the *residual*  $\nabla$ -DB conditions of both directions:  $\nabla_{x_{t+1}} \log \tilde{P}_F(x_{t+1}|x_t) = -\nabla_{x_{t+1}} \log \tilde{P}_F(x_{t+2}|x_{t+1})$ . The bidirectional *residual*  $\nabla$ -DB condition can be analogously understood as the balance condition of two forces from  $x_t$  and  $x_{t+2}$  acting on  $x_{t+1}$ : if not balanced, one can locally find some other  $x_{t+1}$  that makes both transitions more probable.

**Flow reparameterization through forward-looking (FL) trick.** Though mathematically solid, such a bidirectional condition suffers from inefficient credit assignment for long sequences, a problem commonly observed in RL settings [52, 54]. Instead, we may leverage the priors we have from the pretrained diffusion model to speed up the finetuning process, by considering the individual conditions for the forward and reverse directions. Specifically, we employ the forward-looking (FL) technique for GFlowNets [35, 68] and parameterize the residual flow score function with a “baseline” of the “one-step predicted reward gradient”:

$$\nabla_{x_t} \log \tilde{F}(x_t) \triangleq \beta \gamma_t \nabla_{x_t} \log \underbrace{R(\hat{x}_\theta(x_t))}_{\text{predicted reward}} + g_\phi(x_t) \quad (15)$$

where  $\gamma_t$  is the scalar to control the strength of forward looking (with  $\gamma_T = 1$ ) and  $g_\phi(x_t)$  is the actual neural network with parameters  $\phi$  satisfying a terminal constraint  $g_\phi(x_T) = 0$ . Here  $\hat{x}_\theta(\cdot)$  is the one-step clean data prediction defined in Equation 2. This FL technique is to involve a useful external information, which is a partial signal  $\nabla_{x_t} \log R(\hat{x}_\theta(x_t))$  about state  $x_t$ , such that the learning of the flow function becomes easier, as the scale of the difference to its optimal value becomes smaller [35].

We therefore obtain the forward-looking version of *residual*  $\nabla$ -DB losses of both directions:

$$L_{\nabla\check{DB-FL-res}}(x_t, x_{t+1}) = \left\| \nabla_{x_{t+1}} \log \tilde{P}_F(x_{t+1}|x_t; \theta) - \left[ \beta \gamma_t \nabla_{x_{t+1}} \log R(\hat{x}_\theta(x_{t+1})) + g_\phi(x_{t+1}) \right] \right\|^2. \quad (16)$$

$$L_{\nabla\check{DB-FL-res}}(x_t, x_{t+1}) = \left\| \nabla_{x_t} \log \tilde{P}_F(x_{t+1}|x_t) + \left[ \beta \gamma_t \nabla_{x_t} \log R(\hat{x}_\theta(x_t)) + g_\phi(x_t) \right] \right\|^2. \quad (17)$$

What’s more, the corresponding terminal loss objective now becomes

$$L_{\nabla DB-FL-terminal}(x_T) = \left\| \nabla_{x_T} \log \tilde{F}(x_T) - \beta \gamma_t \nabla_{x_T} \log R(x_T) \right\|^2 = \left\| g_\phi(x_T) \right\|^2, \quad (18)$$

which indicates that the actual parameterized flow network  $g_\phi$  should take a near-zero value for terminal states  $x_T$ . The total loss on a collected trajectory  $\tau = (x_1, \dots, x_T)$  is therefore

$$\sum_t \left[ w_F(t) L_{\nabla\check{DB-FL-res}}(x_t, x_{t+1}) + w_B(t) L_{\nabla\check{DB-FL-res}}(x_t, x_{t+1}) \right] + L_{\nabla DB-FL-terminal}(x_T) \quad (19)$$

where  $w_F(t)$  and  $w_B(t)$  are scalar weights to control the relative importance of each term.

We summarize the resulting algorithm in Algorithm 1 in Appendix.

**Choice of FL scale.** Naïvely setting  $\gamma_t = 1$  can be too aggressive especially when the reward scale  $\eta$  and the learning rate are set to a relatively high value. Inspired by the fact that in diffusion models  $F_t(x_t)$  can be seen as  $R(x)$  smoothed with a Gaussian kernel, we propose to set  $\gamma_t = \alpha_{T-t}$ . We compare this design choice with the naïve one in the appendix.

## 270 4 EXPERIMENTS

### 271 4.1 BASELINES

272 For gradient-free methods, we consider DAG-DB [68] (*i.e.*, GFlowNet finetuning with the DB ob-  
 273 jective) and DDPO [5]. Since the original DB objective aims to finetune with  $R^\beta(x)$  instead of  
 274  $P_F^\#(x_T)R^\beta(x_T)$ , we also consider the residual DB loss, defined as

$$275 L_{\text{DB-FL-res}}(x_t, x_{t+1}) = \left( \log \tilde{P}_F(x_{t+1}|x_t) - \beta \log R(\hat{x}_\theta(x_{t+1})) - g(x_{t+1}; \phi) \right)^2. \quad (20)$$

276 For other gradient-aware finetuning methods, we consider ReFL [60] and DRaFT [7]. ReFL samples  
 277 a trajectory and stops some random time step  $t$ , with which it maximizes  $R(\hat{x}_\theta(\nabla(x_t)))$  where  $\hat{x}_\theta(\cdot)$   
 278 is the one-step sample prediction function and  $\nabla$  is the stop-gradient operation. Different from  
 279 ReFL, DRaFT samples some time step  $T - K$  (typically  $K = 1$ ) and expand the computational  
 280 graph of DDPM from  $\nabla(x_{T-K})$  to  $x_T$  so that the reward signal  $R(x_T)$  can be backpropagated to  
 281  $x_{T-K}$ , with all  $x_t$  in the previous time steps removed from this computational graph. A variant  
 282 of DRaFT called DRaFT-LV performs few extra steps of “noising-denoising” on the sampled  $x_T$   
 283 before feeding it into the reward function  $R(\cdot)$ .

### 284 4.2 REWARD FUNCTIONS, PROMPT DATASETS AND METRICS

285 For the main experiments, we consider two reward functions: Aesthetic Score [24], Human Prefer-  
 286 ence Score (HPSv2) [57, 58] and ImageReward [60], all of which trained on large-scale human pref-  
 287 erence datasets such as LAION-aesthetic [24]. For base experiments with Aesthetic Score, we use a  
 288 set of 45 simple animal prompts as used in DDPO [5]; for those with HPSv2, we use photo+painting  
 289 prompts from the human preference dataset (HPDv2) [57]. To measure the diversity of generated  
 290 images, we follow Domingo-Enrich et al. [10] and compute the variance of latent features extracted  
 291 from a batch of generated images (we use a batch of size 64). Using the same set of examples, we  
 292 evaluate the capability of prior following, we compute the per-prompt FID score between images  
 293 generated from the pretrained model and from the finetuned model and take the average FID score  
 294 over all evaluation prompts.

### 295 4.3 EXPERIMENT SETTINGS

296 For all methods, we use 50-step DDPM sampler to construct the MDP. We use StableDiffusion-v1.5  
 297 [41] as the base models. For the finetuned diffusion model policies, we use low-rank adaptation  
 298 (LoRA) [17]. The residual flow score function in *residual*  $\nabla$ -DB is set to be a scaled-down version  
 299 of the StableDiffusion U-Net, whereas the flow function (in DAG-DB and *residual* DB) is set to be a  
 300 similar network but without the U-Net decoding structure (since the desired output is a scalar instead  
 301 of an image vector). Both networks are initialized with tiny weights in the final output layers.

302 As the landscape of  $R(x)$  can be highly non-smooth, we approximate  $\nabla_{x_t} \log R(\hat{x}_\theta(x_t))$   
 303 with  $\mathbb{E}_{\epsilon \sim \mathcal{N}(0, c)} \nabla_{x_t} \log R(\hat{x}_\theta(x_t) + \epsilon)$  where  $c$  is a tiny constant. For StableDiffusion  
 304 [41], since the diffusion process runs in the latent space, the reward function is instead  
 305  $\mathbb{E}_{\epsilon \sim \mathcal{N}(0, c)} \nabla_{x_t} \log R(\text{decode}(\hat{x}_\theta(x_t) + \epsilon))$  in which  $\text{decode}(\cdot)$  is the pretrained (and frozen) VAE  
 306 decoder and  $c$  is set to  $2 \times 10^{-3}$ , slightly smaller than one pixel (*i.e.*,  $1/255$ ). We approximate this  
 307 expectation with 3 independent samples for each transition in each trajectory. For all experiments,  
 308 we try 3 random seeds. Unless otherwise specified, we set  $w_B(t) = 1$ .

309 To stabilize the training process of our method (*residual*  $\nabla$ -DB), we follow the official repo of  
 310 DAG-DB and uses output regularization:  $\lambda \|\epsilon_{\theta^\dagger}(x_t) - \epsilon_{\theta^\ddagger}(x_t)\|^2$  where  $\theta^\dagger$  is the diffusion model  
 311 parameters in the previous update step<sup>5</sup>. We set the output regularization strength  $\lambda = 1000$  in  
 312 Aesthetic Score experiments and  $\lambda = 100$  in HPSv2 experiments. For all experiments with *residual*  
 313  $\nabla$ -DB, we set the learning rate to  $1 \times 10^{-3}$  and ablate over a set of choices of reward temperature  $\beta$ ,  
 314 in a range such that the reward gradients are more significant than the residual policy score function  
 315  $\nabla_{x_t} \log P_F(x_{t+1}|x_t)$  of the pretrained model. For HPSv2 and ImageReward experiments, we set  $\beta$

316 <sup>5</sup>Essentially a Fisher divergence between the pretrained and the finetuned distributions conditioned on  $x_t$ .  
 317 Similar regularization with KL divergence has been seen in popular on-policy RL algorithms like TRPO [44]  
 318 and PPO [45].

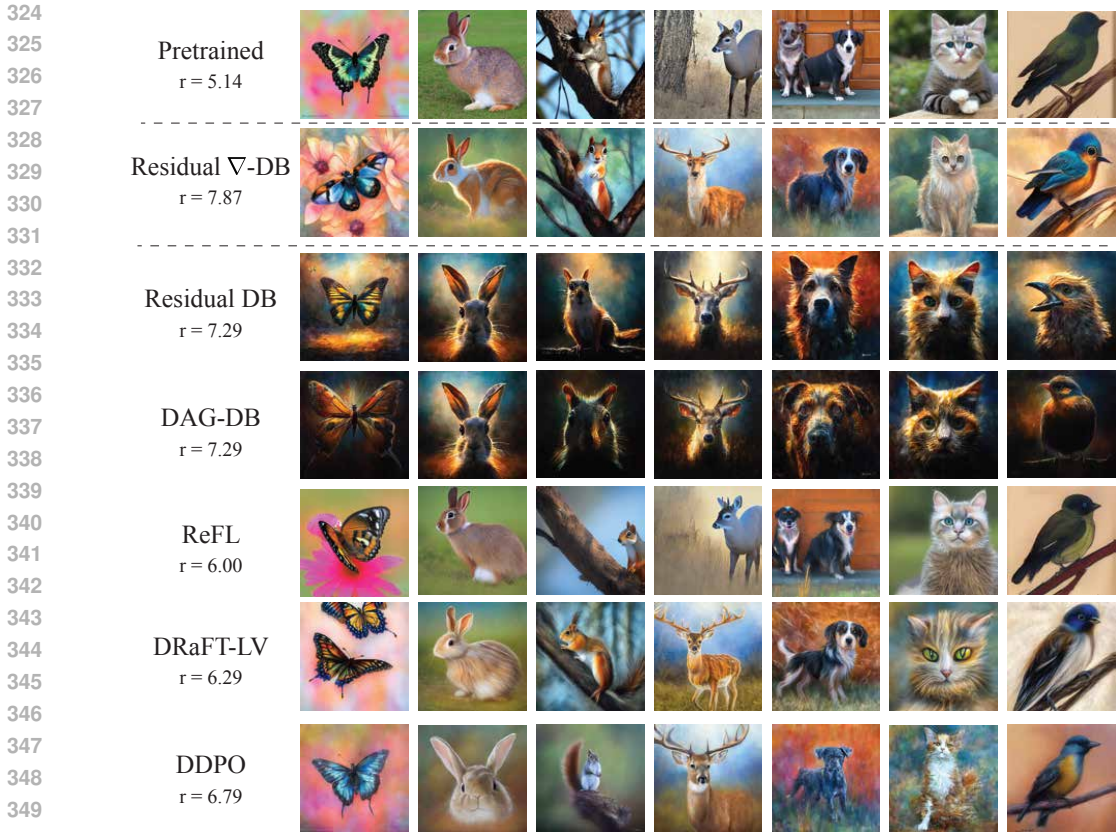


Figure 2: Comparison between images generated by models finetuned with different methods for a maximum of 200 update steps. For each method, we pick the model trained that produces the most visually-appealing figure among all model checkpoints, as methods like ReFL and DRaFT-LV easily collapses (as illustrated in Fig. 3). For each method, we show the average reward of the corresponding presented images.

to be 500000 and 10000, respectively. We always set  $w_F(t) = 1$  for all  $t$ 's and unless otherwise specified we set  $w_b(t) = 1$ . For each epoch, we collect 64 generation trajectories for each of which we randomly shuffle the orders of transitions. We use the number of gradient accumulation steps to 4 and for each 32 trajectories we update both the forward policy and the residual flow score function. For *residual*  $\nabla$ -DB in most of the experiments, we sub-sample 10% of the transitions in each collected trajectory for training by taking one single uniformly sample in uniformly split time-step intervals but ensure that the final transition step always included.

For *residual* DB and DAG-DB, we set the learning rate to  $3 \times 10^{-4}$  with output regularization strength  $\lambda = 1$ . The sampling and training procedures are similar to that of *residual*  $\nabla$ -DB experiments. For ReFL, we follow the official repo and similarly set the random stop time steps to between 35 and 49. For DRaFT, since the official code is not released, we follow the settings in AlignProp [39], a similar concurrent paper. We set the loss for both ReFL and DRaFT to  $-\mathbb{E}_{x_T \sim P_F} \text{ReLU}(R(\text{decode}(x_T)))$  where the ReLU function is introduced for training stability in the case of the ImageReward reward function.

#### 4.4 RESULTS

**General experiments.** In Figure 6 and Table 1, we show the evolution of reward, DreamSim diversity of all methods with the mean curves and the corresponding standard deviations (on 3 random seeds). Our proposed *residual*  $\nabla$ -DB is able to achieve comparable convergence speed, measured in update steps, to that of the gradient-free baselines while those diversity-aware baselines fail to



Figure 3: Finetuning with our  $\nabla$ -GFlowNet is stable compared to other baselines.



378  
379  
380  
381  
382  
383  
384  
385  
386  
387  
388  
389  
390  
391  
392  
393  
394  
395  
396  
397  
398  
399  
400  
401  
402  
403  
404  
405  
406  
407  
408  
409  
410  
411  
412  
413  
414  
415  
416  
417  
418  
419  
420  
421  
422  
423  
424  
425  
426  
427  
428  
429  
430  
431

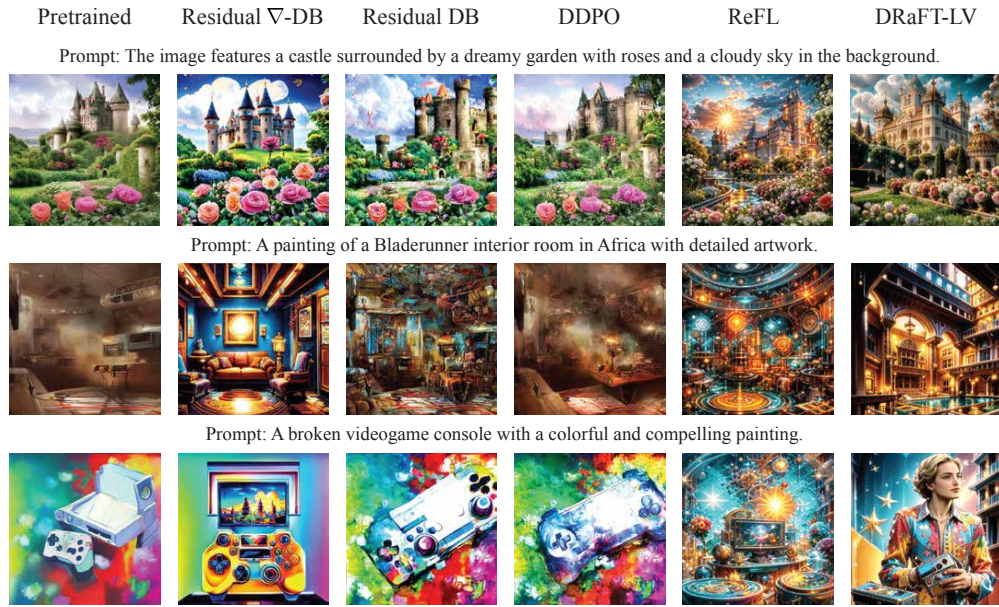


Figure 4: Qualitative results on HPSv2.

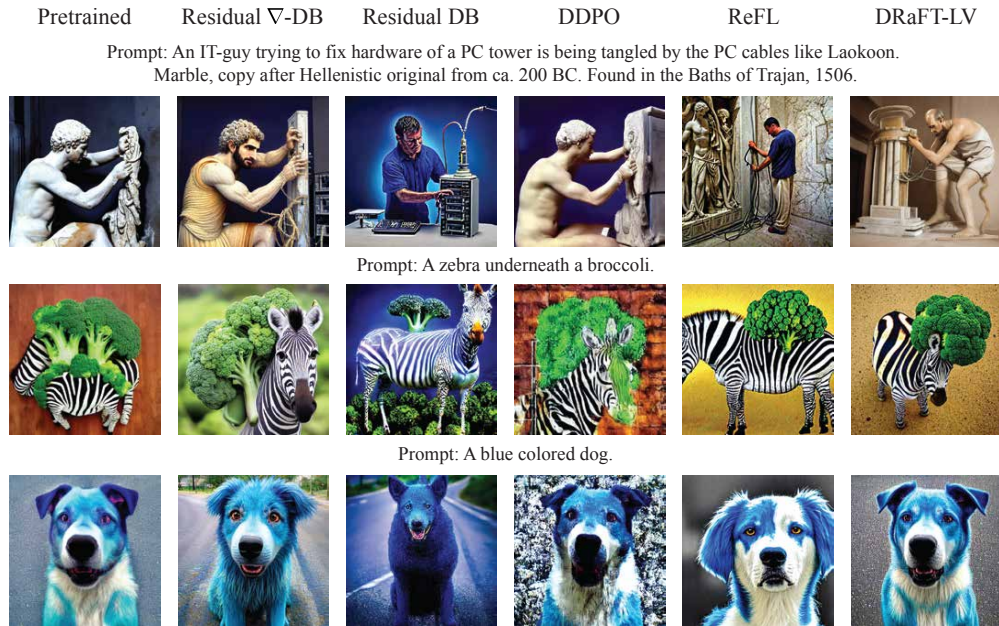


Figure 5: Qualitative results on ImageReward.

do so. In Figure 7, we plot the diversity-reward tuples and FID-reward tuples for models evaluated at different checkpoints (every 5 update steps) and show that our method achieves better trade-off between diversity and reward and between prior-following and reward. The gradient-informed baselines, ReFL and the DRaFT variants, generally behave worse than *residual*  $\nabla$ -DB due to their mode-seeking nature. Qualitatively, we show that the model finetuned with *residual*  $\nabla$ -DB on Aesthetic Score generate more aesthetic and more diverse samples in both style and subject identity (Fig. 2, and Fig. 24 in the appendix), while the other baselines exhibit mode collapse or even catastrophic forgetting of pretrained image prior. We also demonstrate some of the images generated by the diffusion model finetuned with *residual*  $\nabla$ -DB on HPSv2 in Figure 4 and on ImageReward in Figure 5. Furthermore, we qualitatively show that *residual*  $\nabla$ -DB is robust while with the gradient-informed baseline methods are prone to training collapse (Fig. 3). Due to the limited space, we some ablation

Method	Aesthetic Score			HPSv2			ImageReward		
	Reward (↑)	Diversity DreamSim (↑, $10^{-2}$ )	FID (↓)	Reward (↑, $10^{-1}$ )	Diversity DreamSim (↑, $10^{-2}$ )	FID (↓)	Reward (↑, $10^{-1}$ )	Diversity DreamSim (↑, $10^{-2}$ )	FID (↓)
Base Model	5.83±0.01	35.91±0.00	216±1	2.38±0.13	37.75±0.21	563±5	-0.38±0.12	41.09±0.03	468±1
Ours ( $w_B=1$ )	7.90±0.09	<b>29.67</b> ±0.51	317±15	3.53±0.04	24.39±0.87	1000±39	2.23±0.34	<b>39.85</b> ±0.67	<b>501</b> ±7
Ours ( $w_B=0$ )	7.86±0.06	29.21±0.18	318±13	3.53±0.03	24.40±0.56	973±5	5.33±0.62	35.85±0.66	638±15
<i>residual</i> DB	7.20±0.92	19.38±4.07	1065±587	2.55±0.06	32.49±0.47	840±107	<b>6.47</b> ±0.54	25.52±0.35	772±19
DAG-DB	7.73±0.07	15.88±0.70	595±87	2.52±0.06	<b>32.50</b> ±0.59	866±41	4.70±0.75	26.78±0.64	809±34
DDPO	6.68±0.14	32.96±1.04	<b>312</b> ±9	2.52±0.04	3.49±0.03	<b>681</b> ±16	0.27±0.38	38.51±1.49	714±25
ReFL	9.53±0.46	8.20±3.06	1765±51	3.67±0.06	19.84±1.70	1191±46	1.36±0.30	36.50±0.52	597±10
DRaFT-1	10.16±0.13	4.24±0.45	1665±182	3.70±0.06	18.96±1.35	1222±84	1.59±0.25	37.27±0.49	531±13
DRaFT-LV	<b>10.21</b> ±0.34	6.39±1.66	1854±296	<b>3.75</b> ±0.08	21.13±1.19	1164±43	1.44±0.25	37.56±0.09	529±18

Table 1: Comparison between the models finetuned with our proposed method *residual*  $\nabla$ -DB and the baselines. All models are finetuned with 200 update steps. For each method, the model with the best mean reward is used for evaluation. Note that while baselines like DDPO can achieve better scores on some metric, it often comes with the price of much worse performance on some other.

studies to Appendix F, and only show the most important ones in the main text. For the same reason, we also leave plots for experiments on HPSv2 and ImageReward to Appendix E.

**Effect of reward temperature.** We perform ablation study on Aesthetic Score with  $\beta \in \{5000, 7000, 1000\}$  in *residual*  $\nabla$ -DB. Not surprisingly, a higher reward temperature leads to faster convergence at the cost of worse diversity and worse prior-following, as observed in Figure 8.

**Effect of sub-sampling.** Typically, sub-sampling results in worse gradient estimates. We empirically study how sub-sampling may effect the performance and show the results in Figure 10 and ?? in the appendix. We empirically do not observe huge performance drop due to subsampling strategy, potentially because the rich gradient signals in both the reward and the flow are sufficient.

**Effect of different prior strengths.** We experiment with choices of prior strengths  $\eta$  and observed in Fig. 16 and 17 that lower  $\eta$  lead to better diversity-reward trade-off and faster reward convergence.

**Reward finetuning with other sampling algorithms.** To show that our method generalizes to different sampling diffusion algorithms, we construct another MDP based on SDE-DPM-Solver++ [30], with 20 inference steps. In Fig. 18 and 19, we observe that our *residual*  $\nabla$ -DB can still achieve a good balance between reward convergence speed, diversity preservation and prior following.

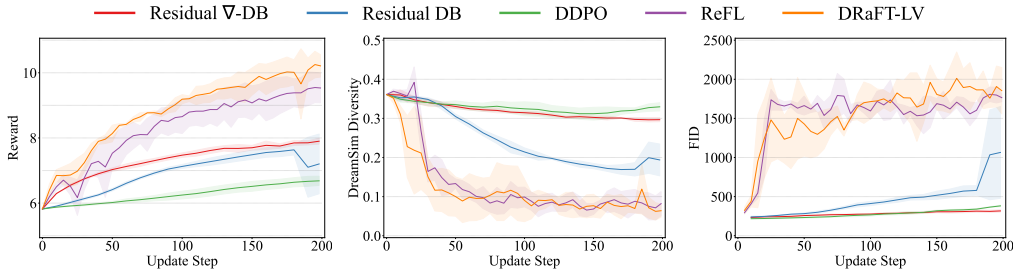


Figure 6: Convergence curves of different metrics for different methods throughout the finetuning process on Aesthetic Score. Finetuning with our proposed *residual*  $\nabla$ -DB converges faster than the non-gradient-informed methods and with better diversity-preserving and prior-following capability.

## 5 RELATED WORK

**Reward finetuning of diffusion models.** The demand for reward finetuning is probably most commonly seen in alignment, where one obtains utilize a human reference reward function to align the behavior of generative models [18, 1, 57] for better instruction following capability and better AI safety. With a reward function, typically obtained by learning from human preference datasets [72, 51], one may use reinforcement learning (RL) algorithms, for instance PPO [45], to

486  
487  
488  
489  
490  
491  
492  
493  
494  
495  
496

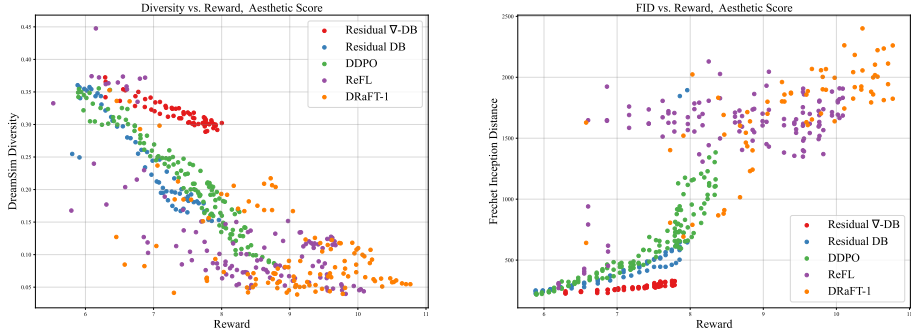


Figure 7: Trade-offs between reward, diversity and priority following (measured by FID) for different reward finetuning methods. Dots represent the evaluation results of models checkpoint saved after every 5 iterations of finetuning, where ones with larger reward, larger diversity scores and smaller FID scores are considered better.

500  
501  
502  
503  
504  
505  
506  
507  
508

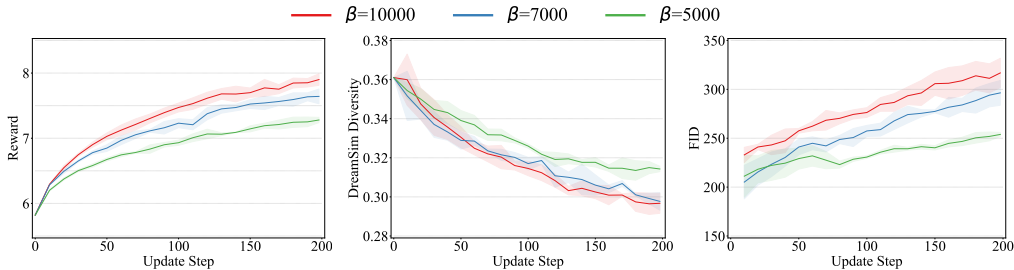


Figure 8: Higher temperature  $\beta$  leads to faster convergence but with less diversity and less prior following.

509  
510  
511  
512  
513  
514  
515  
516  
517  
518  
519  
520  
521  
522  
523  
524  
525  
526  
527  
528  
529  
530  
531  
532

adapt not only autoregressive language models [34] which naturally admits a Markov decision process (MDP), but also diffusion models [5, 12]. Specifically, one can construct MDPs from some diffusion sampling algorithm [48, 30] by considering each noisy image at some inference step as a state and each denoising step as an action. Besides RL algorithms, there exist some other approaches, including stochastic optimal control [10, 53], GFlowNets [68] and some other ones akin to RL methods [26, 11]. While most of the aforementioned approaches train with only black-box rewards, once we have access to a differentiable reward function we may accelerate the finetuning process with reward gradient signals. For instance, methods exist to construct a computational graph from sampled generation trajectories to directly optimize for rewards [7, 39, 59], yet with these methods models are not trained to correctly sample according to the reward function. While one may also generate samples from the reward function without finetuning using plug-in guidance methods for diffusion models [9, 49, 22, 13] as an alternative, but the generated distributions are often very biased. Besides, reward finetuning for diffusion models is typically memory consuming as many methods require a large computational graph rolled out from long generation trajectories, for which it is typical to employ efficient finetuning techniques [17, 40, 27].

**GFlowNets.** Generative flow network [3], or GFlowNet in short, is a high-level algorithmic framework that introduces sequential decision-making into generative modeling [63], bridging methodology between reinforcement learning [66, 36, 37, 35, 25] and energy-based modeling [64]. GFlowNets perform amortized variational inference [32] and generate samples with probability proportional to a given density or reward function, in contrast to the typical reward maximization objective in reinforcement learning. GFlowNets can therefore be used to generate high-quality and diverse samples for applications including but not limited to drug discovery [19, 20, 46], structure learning [8], phylogenetic inference [71] and combinatorial optimization [62, 65].

## 6 CONCLUSION

533  
534  
535  
536  
537  
538  
539

We propose  $\nabla$ -GFlowNet, a fast, diversity-preserving and prior-following reward finetuning method for diffusion models, by leveraging gradient information in the probabilistic framework of GFlowNets that aims to sample according to a given unnormalized density function. Our empirical results show that  $\nabla$ -GFlowNet achieves a better trade-off between convergence speed, diversity in generated samples and prior following. We hope that our method sheds lights on future studies on more efficient reward finetuning strategies of diffusion models as well as related applications.

## REFERENCES

- [1] Yuntao Bai, Andy Jones, Kamal Ndousse, Amanda Askell, Anna Chen, Nova DasSarma, Dawn Drain, Stanislav Fort, Deep Ganguli, Tom Henighan, Nicholas Joseph, Saurav Kadavath, Jackson Kernion, Tom Conerly, Sheer El-Showk, Nelson Elhage, Zac Hatfield-Dodds, Danny Hernandez, Tristan Hume, Scott Johnston, Shauna Kravec, Liane Lovitt, Neel Nanda, Catherine Olsson, Dario Amodei, Tom Brown, Jack Clark, Sam McCandlish, Chris Olah, Ben Mann, and Jared Kaplan. Training a helpful and harmless assistant with reinforcement learning from human feedback, 2022.
- [2] Emmanuel Bengio, Moksh Jain, Maksym Korablyov, Doina Precup, and Yoshua Bengio. Flow network based generative models for non-iterative diverse candidate generation. In *Advances in Neural Information Processing Systems*, 2021.
- [3] Yoshua Bengio, Salem Lahlou, Tristan Deleu, Edward J Hu, Mo Tiwari, and Emmanuel Bengio. GFlowNet foundations. *Journal of Machine Learning Research*, (24):1–76, 2023.
- [4] Yoshua Bengio, Salem Lahlou, Tristan Deleu, Edward J Hu, Mo Tiwari, and Emmanuel Bengio. Gflownet foundations. *The Journal of Machine Learning Research*, 24(1):10006–10060, 2023.
- [5] Kevin Black, Michael Janner, Yilun Du, Ilya Kostrikov, and Sergey Levine. Training diffusion models with reinforcement learning. In *International Conference on Learning Representations*, 2024.
- [6] Paul Christiano, Jan Leike, Tom Brown, Miljan Martic, Shane Legg, and Dario Amodei. Deep reinforcement learning from human preferences. In *Advances in Neural Information Processing Systems*, volume 30, 2017.
- [7] Kevin Clark, Paul Vicol, Kevin Swersky, and David J. Fleet. Directly fine-tuning diffusion models on differentiable rewards. In *International Conference on Learning Representations*, 2024.
- [8] Tristan Deleu, António Góis, Chris Emezue, Mansi Rankawat, Simon Lacoste-Julien, Stefan Bauer, and Yoshua Bengio. Bayesian structure learning with generative flow networks. *Uncertainty in Artificial Intelligence (UAI)*, 2022.
- [9] Prafulla Dhariwal and Alexander Nichol. Diffusion models beat gans on image synthesis. In *Advances in neural information processing systems*, 2021.
- [10] Carles Domingo-Enrich, Michal Drozdal, Brian Karrer, and Ricky T. Q. Chen. Adjoint matching: Fine-tuning flow and diffusion generative models with memoryless stochastic optimal control. *arXiv preprint arXiv:2409.08861*, 2024.
- [11] Hanze Dong, Wei Xiong, Deepanshu Goyal, Yihan Zhang, Winnie Chow, Rui Pan, Shizhe Diao, Jipeng Zhang, Kashun Shum, and Tong Zhang. Raft: Reward ranked finetuning for generative foundation model alignment, 2023.
- [12] Ying Fan, Olivia Watkins, Yuqing Du, Hao Liu, Moonkyung Ryu, Craig Boutilier, P. Abbeel, Mohammad Ghavamzadeh, Kangwook Lee, and Kimin Lee. Dpok: Reinforcement learning for fine-tuning text-to-image diffusion models. *ArXiv*, abs/2305.16381, 2023.
- [13] Yingqing Guo, Hui Yuan, Yukang Yang, Minshuo Chen, and Mengdi Wang. Gradient guidance for diffusion models: An optimization perspective, 2024. URL <https://arxiv.org/abs/2404.14743>.
- [14] Jonathan Ho, Ajay Jain, and Pieter Abbeel. Denoising diffusion probabilistic models. In *Advances in neural information processing systems*, 2020.
- [15] Jonathan Ho, Tim Salimans, Alexey Gritsenko, William Chan, Mohammad Norouzi, and David J Fleet. Video diffusion models. *Advances in Neural Information Processing Systems*, 35, 2022.



- 594 [16] Emiel Hoogeboom, Victor Garcia Satorras, Clément Vignac, and Max Welling. Equivariant  
595 diffusion for molecule generation in 3d. In *International conference on machine learning*,  
596 2022.
- 597 [17] Edward J Hu, Yelong Shen, Phillip Wallis, Zeyuan Allen-Zhu, Yuanzhi Li, Shean Wang,  
598 Lu Wang, and Weizhu Chen. LoRA: Low-rank adaptation of large language models. In *Inter-  
599 national Conference on Learning Representations*, 2022.
- 600 [18] Borja Ibarz, Jan Leike, Tobias Pohlen, Geoffrey Irving, Shane Legg, and Dario Amodei. Re-  
601 ward learning from human preferences and demonstrations in atari, 2018.
- 602 [19] Moksh Jain, Emmanuel Bengio, Alex Hernandez-Garcia, Jarrid Rector-Brooks, Bonaven-  
603 ture F.P. Dossou, Chanakya Ekbote, Jie Fu, Tianyu Zhang, Micheal Kilgour, Dinghuai Zhang,  
604 Lena Simine, Payel Das, and Yoshua Bengio. Biological sequence design with GFlowNets.  
605 *International Conference on Machine Learning (ICML)*, 2022.
- 606 [20] Moksh Jain, Tristan Deleu, Jason S. Hartford, Cheng-Hao Liu, Alex Hernández-García, and  
607 Yoshua Bengio. Gflownets for ai-driven scientific discovery. *ArXiv*, abs/2302.00615, 2023.  
608 URL <https://api.semanticscholar.org/CorpusID:256459319>.
- 609 [21] Oliver Johnson. *Information theory and the central limit theorem*. World Scientific, 2004.
- 610 [22] Lingkai Kong, Yuanqi Du, Wenhao Mu, Kirill Neklyudov, Valentin De Bortol, Haorui Wang,  
611 Dongxia Wu, Aaron Ferber, Yi-An Ma, Carla P Gomes, et al. Diffusion models as constrained  
612 samplers for optimization with unknown constraints. *arXiv preprint arXiv:2402.18012*, 2024.
- 613 [23] Salem Lahlou, Tristan Deleu, Pablo Lemos, Dinghuai Zhang, Alexandra Volokhova, Alex  
614 Hernández-García, Léna Néhale Ezzine, Yoshua Bengio, and Nikolay Malkin. A theory of  
615 continuous generative flow networks. *International Conference on Machine Learning (ICML)*,  
616 2023.
- 617 [24] LAION. Laion aesthetic score predictor. [https://laion.ai/blog/  
618 laion-aesthetics/](https://laion.ai/blog/laion-aesthetics/), 2024. Accessed: 2024-09-27.
- 619 [25] Elaine Lau, Stephen Zhewen Lu, Ling Pan, Doina Precup, and Emmanuel Bengio. Qgfn: Con-  
620 trollable greediness with action values, 2024. URL [https://arxiv.org/abs/2402.  
621 05234](https://arxiv.org/abs/2402.05234).
- 622 [26] Kimin Lee, Hao Liu, Moonkyung Ryu, Olivia Watkins, Yuqing Du, Craig Boutilier, P. Abbeel,  
623 Mohammad Ghavamzadeh, and Shixiang Shane Gu. Aligning text-to-image models using  
624 human feedback. *ArXiv*, abs/2302.12192, 2023.
- 625 [27] Weiyang Liu, Zeju Qiu, Yao Feng, Yuliang Xiu, Yuxuan Xue, Longhui Yu, Haiwen Feng, Zhen  
626 Liu, Juyeon Heo, Songyou Peng, et al. Parameter-efficient orthogonal finetuning via butterfly  
627 factorization. In *International Conference on Learning Representations*, 2024.
- 628 [28] Zhen Liu, Yao Feng, Michael J Black, Derek Nowrouzezahrai, Liam Paull, and Weiyang Liu.  
629 Meshdiffusion: Score-based generative 3d mesh modeling. In *International Conference on  
630 Learning Representations*, 2023.
- 631 [29] Zhen Liu, Yao Feng, Yuliang Xiu, Weiyang Liu, Liam Paull, Michael J Black, and Bernhard  
632 Schölkopf. Ghost on the shell: An expressive representation of general 3d shapes. In *Inter-  
633 national Conference on Learning Representations*, 2024.
- 634 [30] Cheng Lu, Yuhao Zhou, Fan Bao, Jianfei Chen, Chongxuan Li, and Jun Zhu. Dpm-solver: A  
635 fast ode solver for diffusion probabilistic model sampling in around 10 steps. In *ICLR*, 2023.
- 636 [31] Nikolay Malkin, Moksh Jain, Emmanuel Bengio, Chen Sun, and Yoshua Bengio. Trajectory  
637 balance: Improved credit assignment in gflownets. In *Advances in Neural Information Pro-  
638 cessing Systems*, 2022.
- 639 [32] Nikolay Malkin, Salem Lahlou, Tristan Deleu, Xu Ji, Edward Hu, Katie Everett, Dinghuai  
640 Zhang, and Yoshua Bengio. GFlowNets and variational inference. *International Conference  
641 on Learning Representations (ICLR)*, 2023.



- 648 [33] Azalia Mirhoseini, Anna Goldie, Mustafa Yazgan, Joe Jiang, Ebrahim Songhori, Shen Wang,  
649 Young-Joon Lee, Eric Johnson, Omkar Pathak, Sungmin Bae, et al. Chip placement with deep  
650 reinforcement learning. *arXiv preprint arXiv:2004.10746*, 2020.
- 651 [34] Long Ouyang, Jeffrey Wu, Xu Jiang, Diogo Almeida, Carroll Wainwright, Pamela Mishkin,  
652 et al. Training language models to follow instructions with human feedback. *arXiv preprint*  
653 *arXiv:2203.02155*, 2022.
- 654 [35] Ling Pan, Nikolay Malkin, Dinghuai Zhang, and Yoshua Bengio. Better training of gflownets  
655 with local credit and incomplete trajectories. In *International Conference on Machine Learn-*  
656 *ing*, 2023.
- 657 [36] Ling Pan, Dinghuai Zhang, Aaron Courville, Longbo Huang, and Yoshua Bengio. Generative  
658 augmented flow networks. *International Conference on Learning Representations (ICLR)*,  
659 2023.
- 660 [37] Ling Pan, Dinghuai Zhang, Moksh Jain, Longbo Huang, and Yoshua Bengio. Stochastic gen-  
661 erative flow networks. *Uncertainty in Artificial Intelligence (UAI)*, 2023.
- 662 [38] Ben Poole, Ajay Jain, Jonathan T Barron, and Ben Mildenhall. Dreamfusion: Text-to-3d using  
663 2d diffusion. In *International Conference on Learning Representations*, 2023.
- 664 [39] Mihir Prabhudesai, Anirudh Goyal, Deepak Pathak, and Katerina Fragkiadaki. Aligning text-  
665 to-image diffusion models with reward backpropagation. *arXiv preprint arXiv:2310.03739*,  
666 2023.
- 667 [40] Zeju Qiu, Weiyang Liu, Haiwen Feng, Yuxuan Xue, Yao Feng, Zhen Liu, Dan Zhang, Adrian  
668 Weller, and Bernhard Schölkopf. Controlling text-to-image diffusion by orthogonal finetuning.  
669 In *Advances in Neural Information Processing Systems*, 2023.
- 670 [41] Robin Rombach, Andreas Blattmann, Dominik Lorenz, Patrick Esser, and Björn Ommer.  
671 High-resolution image synthesis with latent diffusion models. In *Proceedings of the IEEE/CVF*  
672 *conference on computer vision and pattern recognition*, 2022.
- 673 [42] Olaf Ronneberger, Philipp Fischer, and Thomas Brox. U-net: Convolutional networks for  
674 biomedical image segmentation, 2015. URL <https://arxiv.org/abs/1505.04597>.
- 675 [43] Chitwan Saharia, William Chan, Saurabh Saxena, Lala Li, Jay Whang, Emily L Denton, Kam-  
676 yar Ghasemipour, Raphael Gontijo Lopes, Burcu Karagol Ayan, Tim Salimans, et al. Pho-  
677 torealtistic text-to-image diffusion models with deep language understanding. In *Advances in*  
678 *neural information processing systems*, 2022.
- 679 [44] John Schulman, Sergey Levine, Pieter Abbeel, Michael Jordan, and Philipp Moritz. Trust  
680 region policy optimization. In *ICML*, 2015.
- 681 [45] John Schulman, Filip Wolski, Prafulla Dhariwal, Alec Radford, and Oleg Klimov. Proximal  
682 policy optimization algorithms. *arXiv preprint arXiv:1707.06347*, 2017.
- 683 [46] Max W. Shen, Emmanuel Bengio, Ehsan Hajiramezanali, Andreas Loukas, Kyunghyun Cho,  
684 and Tommaso Biancalani. Towards understanding and improving gflownet training. *ArXiv*,  
685 [abs/2305.07170](https://api.semanticscholar.org/CorpusID:258676487), 2023. URL [https://api.semanticscholar.org/CorpusID:](https://api.semanticscholar.org/CorpusID:258676487)  
686 [258676487](https://api.semanticscholar.org/CorpusID:258676487).
- 687 [47] David Silver, Aja Huang, Chris J. Maddison, Arthur Guez, L. Sifre, George van den Driessche,  
688 Julian Schrittwieser, Ioannis Antonoglou, Vedavyas Panneershelvam, Marc Lanctot, Sander  
689 Dieleman, Dominik Grewe, John Nham, Nal Kalchbrenner, Ilya Sutskever, Timothy P. Lilli-  
690 crap, Madeleine Leach, Koray Kavukcuoglu, Thore Graepel, and Demis Hassabis. Mastering  
691 the game of go with deep neural networks and tree search. *Nature*, 529:484–489, 2016. URL  
692 <https://api.semanticscholar.org/CorpusID:515925>.
- 693 [48] Jiaming Song, Chenlin Meng, and Stefano Ermon. Denoising diffusion implicit models. In  
694 *International Conference on Learning Representations*, 2021.

- 702 [49] Jiaming Song, Qinsheng Zhang, Hongxu Yin, Morteza Mardani, Ming-Yu Liu, Jan Kautz,  
703 Yongxin Chen, and Arash Vahdat. Loss-guided diffusion models for plug-and-play controllable  
704 generation. In *International Conference on Machine Learning*, 2023.  
705
- 706 [50] Yang Song, Jascha Sohl-Dickstein, Diederik P Kingma, Abhishek Kumar, Stefano Ermon, and  
707 Ben Poole. Score-based generative modeling through stochastic differential equations. In  
708 *International Conference on Learning Representations*, 2021.
- 709 [51] Nisan Stiennon, Long Ouyang, Jeff Wu, Daniel M. Ziegler, Ryan Lowe, Chelsea Voss, Alec  
710 Radford, Dario Amodei, and Paul Christiano. Learning to summarize from human feedback,  
711 2022. URL <https://arxiv.org/abs/2009.01325>.  
712
- 713 [52] Richard S. Sutton. Learning to predict by the methods of temporal differences. *Machine*  
714 *Learning*, 3:9–44, 1988.
- 715 [53] Masatoshi Uehara, Yulai Zhao, Kevin Black, Ehsan Hajiramezani, Gabriele Scalia,  
716 Nathaniel Lee Diamant, Alex M Tseng, Tommaso Biancalani, and Sergey Levine. Fine-  
717 tuning of continuous-time diffusion models as entropy-regularized control. *arXiv preprint*  
718 *arXiv:2402.15194*, 2024.
- 719 [54] Hado van Hasselt, Yotam Doron, Florian Strub, Matteo Hessel, Nicolas Sonnerat, and Joseph  
720 Modayil. Deep reinforcement learning and the deadly triad, 2018. URL <https://arxiv.org/abs/1812.02648>.  
721
- 722 [55] Siddharth Venkatraman, Moksh Jain, Luca Scimeca, Minsu Kim, Marcin Sendera, Mohsin  
723 Hasan, Luke Rowe, Sarthak Mittal, Pablo Lemos, Emmanuel Bengio, et al. Amortizing  
724 intractable inference in diffusion models for vision, language, and control. *arXiv preprint*  
725 *arXiv:2405.20971*, 2024.  
726
- 727 [56] Luhuan Wu, Brian Trippe, Christian Naeseth, David Blei, and John P Cunningham. Practical  
728 and asymptotically exact conditional sampling in diffusion models. In *Advances in Neural*  
729 *Information Processing Systems*, 2024.  
730
- 731 [57] Xiaoshi Wu, Yiming Hao, Keqiang Sun, Yixiong Chen, Feng Zhu, Rui Zhao, and Hongsheng  
732 Li. Human preference score v2: A solid benchmark for evaluating human preferences of text-  
733 to-image synthesis. *arXiv preprint arXiv:2306.09341*, 2023.
- 734 [58] Xiaoshi Wu, Keqiang Sun, Feng Zhu, Rui Zhao, and Hongsheng Li. Human preference score:  
735 Better aligning text-to-image models with human preference. In *Proceedings of the IEEE/CVF*  
736 *International Conference on Computer Vision*, 2023.  
737
- 738 [59] Jiazheng Xu, Xiao Liu, Yuchen Wu, Yuxuan Tong, Qinkai Li, Ming Ding, Jie Tang, and Yuxiao  
739 Dong. Imagereward: Learning and evaluating human preferences for text-to-image generation.  
740 *ArXiv*, abs/2304.05977, 2023.
- 741 [60] Jiazheng Xu, Xiao Liu, Yuchen Wu, Yuxuan Tong, Qinkai Li, Ming Ding, Jie Tang, and Yuxiao  
742 Dong. Imagereward: Learning and evaluating human preferences for text-to-image generation.  
743 In *Advances in Neural Information Processing Systems*, 2024.
- 744 [61] Minkai Xu, Lantao Yu, Yang Song, Chence Shi, Stefano Ermon, and Jian Tang. Geodiff: A  
745 geometric diffusion model for molecular conformation generation. In *International Conference*  
746 *on Learning Representations*, 2022.  
747
- 748 [62] David W. Zhang, Corrado Rainone, Markus F. Peschl, and Roberto Bondesan. Robust  
749 scheduling with gflownets. *ArXiv*, abs/2302.05446, 2023. URL <https://api.semanticscholar.org/CorpusID:256827133>.  
750
- 751 [63] Dinghuai Zhang, Ricky T. Q. Chen, Nikolay Malkin, and Yoshua Bengio. Unifying generative  
752 models with GFlowNets and beyond. *arXiv preprint arXiv:2209.02606v2*, 2022.  
753
- 754 [64] Dinghuai Zhang, Nikolay Malkin, Zhen Liu, Alexandra Volokhova, Aaron Courville, and  
755 Yoshua Bengio. Generative flow networks for discrete probabilistic modeling. In *International Conference on Machine Learning*, 2022.

- 756 [65] Dinghui Zhang, Hanjun Dai, Nikolay Malkin, Aaron C. Courville, Yoshua Bengio, and Ling  
757 Pan. Let the flows tell: Solving graph combinatorial optimization problems with gflownets.  
758 *ArXiv*, abs/2305.17010, 2023.
- 759 [66] Dinghui Zhang, L. Pan, Ricky T. Q. Chen, Aaron C. Courville, and Yoshua Bengio. Distribu-  
760 tional gflownets with quantile flows. *arXiv preprint arXiv:2302.05793*, 2023.
- 761 [67] Dinghui Zhang, Ricky T. Q. Chen, Cheng-Hao Liu, Aaron Courville, and Yoshua Bengio.  
762 Diffusion generative flow samplers: Improving learning signals through partial trajectory op-  
763 timization, 2024.
- 764 [68] Dinghui Zhang, Yizhe Zhang, Jiatao Gu, Ruixiang Zhang, Josh Susskind, Navdeep Jaitly, and  
765 Shuangfei Zhai. Improving gflownets for text-to-image diffusion alignment. *arXiv preprint*  
766 *arXiv:2406.00633*, 2024.
- 767 [69] Longwen Zhang, Ziyu Wang, Qixuan Zhang, Qiwei Qiu, Anqi Pang, Haoran Jiang, Wei Yang,  
768 Lan Xu, and Jingyi Yu. Clay: A controllable large-scale generative model for creating high-  
769 quality 3d assets. *ACM Transactions on Graphics (TOG)*, 43(4):1–20, 2024.
- 770 [70] Stephen Zhao, Rob Brekelmans, Alireza Makhzani, and Roger Baker Grosse. Probabilistic  
771 inference in language models via twisted sequential monte carlo. In *International Conference*  
772 *on Machine Learning*, 2024.
- 773 [71] Mingyang Zhou, Zichao Yan, Elliot Layne, Nikolay Malkin, Dinghui Zhang, Moksh Jain,  
774 Mathieu Blanchette, and Yoshua Bengio. Phylogfn: Phylogenetic inference with generative  
775 flow networks, 2024.
- 776 [72] Daniel M. Ziegler, Nisan Stiennon, Jeffrey Wu, Tom B. Brown, Alec Radford, Dario Amodei,  
777 Paul Christiano, and Geoffrey Irving. Fine-tuning language models from human preferences,  
778 2020. URL <https://arxiv.org/abs/1909.08593>.
- 779  
780  
781  
782  
783  
784  
785  
786  
787  
788  
789  
790  
791  
792  
793  
794  
795  
796  
797  
798  
799  
800  
801  
802  
803  
804  
805  
806  
807  
808  
809

# Appendix

## Table of Contents

---

<b>A</b>	<b>Algorithm</b>	<b>17</b>
<b>B</b>	<b>Algorithmic details</b>	<b>17</b>
B.1	$\nabla$ -DB objective as a statistical divergence . . . . .	17
B.2	Proof of Proposition 1 . . . . .	17
B.3	Proof of Proposition 4 . . . . .	18
B.4	Relationship between residual DB and Trajectory Balance . . . . .	19
<b>C</b>	<b>Corrections for non-ideal pretrained models</b>	<b>19</b>
<b>D</b>	<b>Finetuning Convergence in Wall Time</b>	<b>20</b>
<b>E</b>	<b>Figures for ablation results</b>	<b>21</b>
<b>F</b>	<b>Additional ablation experiments</b>	<b>24</b>
<b>G</b>	<b>More samples (Aesthetic Score)</b>	<b>26</b>
<b>H</b>	<b>More samples (HPSv2)</b>	<b>27</b>

---

## A ALGORITHM

---

### Algorithm 1 Diffusion Finetuning with *residual* $\nabla$ -DB

---

- 1: **Inputs:** Pretrained diffusion model  $f_{\theta^\#}$ , reward function  $R(\cdot)$ .
  - 2: **Initialization:** Model to finetune  $f_\theta$  with  $\theta = \theta^\#$ , residual flow score function  $g_\phi(\cdot)$ .
  - 3: Sample the initial batch of trajectories  $\mathcal{D}_{\text{prev}} = \{(x_1, \dots, x_T)_i\}_{i=1\dots N}$  with the current finetuned diffusion model  $f_\theta$ .
  - 4: **while** not converged **do**
  - 5:   Sample a batch of trajectories  $\mathcal{D}_{\text{curr}} = \{(x_1, \dots, x_T)_i\}_{i=1\dots N}$  with the finetuned diffusion model.
  - 6:   Subsample the time steps to train with: the full set  $\mathcal{T}_i = \{1, \dots, T\}$  or the sampled set  $\mathcal{T}_i = \text{Sample-N}(\{1, \dots, T\})$ .
  - 7:   Compute the loss  

$$\sum_{t \in \mathcal{T}_i, (x_{1:T})_i \in \mathcal{D}_{\text{prev}}} L_{\nabla\text{DB-FL-res}}(x_t, x_{t+1}; \theta, \theta^\#, \phi) + L_{\nabla\text{DB-FL-terminal}}(x_T; \phi) + \lambda \|f_\theta(x_t) - f_{\theta^\#}(x_t)\|^2.$$
  - 8:   Update the diffusion model and the residual flow score function.
  - 9:   Set  $\mathcal{D}_{\text{prev}} \leftarrow \mathcal{D}_{\text{curr}}$ .
  - 10: **end while**
  - 11: **return** finetuned model  $f_\theta$ .
- 

## B ALGORITHMIC DETAILS

### B.1 $\nabla$ -DB OBJECTIVE AS A STATISTICAL DIVERGENCE

$L_{\nabla\text{DB}}$  (Equation 7) is analogous to a Fisher divergence (up to a constant scale) if we always use on-policy samples to update the diffusion model and the flow function:

$$\begin{aligned}
 D_{\text{Fisher}}\left(P_F(x_{t+1}|x_t)\right) & \left\| \frac{P_B(x_t|x_{t+1})F(x_{t+1})}{F(x_t)} \right\| \\
 &= \frac{1}{2} \mathbb{E}_{x_{t+1} \sim P_F(x_{t+1}|x_t)} \left\| \nabla_{x_{t+1}} \log P_B(x_t|x_{t+1}) - \nabla_{x_{t+1}} \log \frac{P_B(x_t|x_{t+1})F(x_{t+1})}{F(x_t)} \right\|^2 \\
 &= \frac{1}{2} \mathbb{E}_{x_{t+1} \sim P_F(x_{t+1}|x_t)} L_{\nabla\text{DB}}(x_t, x_{t+1}).
 \end{aligned} \tag{21}$$

### B.2 PROOF OF PROPOSITION 1

*Proof.* When the training objectives equal 0 for all states, we would have

$$\nabla_{x_{t+1}} \log P_F(x_{t+1}|x_t) = \nabla_{x_{t+1}} \log P_B(x_t|x_{t+1}) + \nabla_{x_{t+1}} \log F_{t+1}(x_{t+1}) \tag{22}$$

$$\nabla_{x_t} \log P_F(x_{t+1}|x_t) = \nabla_{x_t} \log P_B(x_t|x_{t+1}) - \nabla_{x_t} \log F_t(x_t) \tag{23}$$

$$\nabla_{x_T} \log F(x_T) = \beta \nabla_{x_T} \log R(x_T) \tag{24}$$

for any trajectory  $(x_0, \dots, x_T)$ .

Through indefinite integral, these indicate that there exist a function  $C_t(x_t)$  satisfies

$$C_t(x_t)P_F(x_{t+1}|x_t) = F_{t+1}(x_{t+1})P_B(x_t|x_{t+1}) \tag{25}$$

$$F_t(x_t)P_F(x_{t+1}|x_t) = C_{t+1}(x_{t+1})P_B(x_t|x_{t+1}) \tag{26}$$

$$F(x_T) \propto R(x_T)^\beta. \tag{27}$$

Therefore, we have

$$\frac{C_t(x_t)}{F_t(x_t)} = \frac{F_{t+1}(x_{t+1})}{C_{t+1}(x_{t+1})}, \quad \forall (x_t, x_{t+1}). \tag{28}$$

The right hand side does not depend on  $x_t$ , therefore, the left hand side is a constant. So we have

$$C_t(x_t) \propto F_t(x_t), \quad \forall t. \tag{29}$$

The probability of generating a data  $x_T$  then equals

$$P_F(x_T) = \int P_0(x_0|\odot) \prod_t P_F(x_{t+1}|x_t) dx_{0:T-1} \quad (30)$$

$$= \int F_0(x_0) \prod_t \frac{F_{t+1}(x_{t+1})P_B(x_t|x_{t+1})}{C_t(x_t)} dx_{0:T-1} \quad (31)$$

$$\propto \int F_0(x_0) \prod_t \frac{F_{t+1}(x_{t+1})P_B(x_t|x_{t+1})}{F_t(x_t)} dx_{0:T-1} \quad (32)$$

$$\propto F(x_T) \int \prod_t P_B(x_t|x_{t+1}) dx_{0:T-1} \quad (33)$$

$$\propto F(x_T) \propto R(x_T)^\beta, \quad (34)$$

which proves the validness of the  $\nabla$ -GFlowNet algorithm.  $\square$

### B.3 PROOF OF PROPOSITION 4

When the training objectives equal 0 for all states, we have

$$\nabla_{x_{t+1}} \log \tilde{P}_F(x_{t+1}|x_t) = \nabla_{x_{t+1}} \log \tilde{F}(x_{t+1}) \quad (35)$$

$$\nabla_{x_t} \log \tilde{P}_F(x_{t+1}|x_t) = -\nabla_{x_t} \log \tilde{F}(x_t) \quad (36)$$

$$\nabla_{x_T} \log \tilde{F}(x_T) = \beta \nabla_{x_T} \log R(x_T) \quad (37)$$

for any trajectory  $(x_0, \dots, x_T)$ .

Through indefinite integral, these indicate that there exist a function  $C_t(x_t)$  satisfies

$$C_t(x_t) \tilde{P}_F(x_{t+1}|x_t) = \tilde{F}(x_{t+1}) \quad (38)$$

$$\tilde{F}(x_t) \tilde{P}_F(x_{t+1}|x_t) = C_{t+1}(x_{t+1}) \quad (39)$$

$$\tilde{F}(x_T) \propto R(x_T)^\beta. \quad (40)$$

Thus we have

$$\frac{C_t(x_t)}{\tilde{F}_t(x_t)} = \frac{\tilde{F}_{t+1}(x_{t+1})}{C_{t+1}(x_{t+1})}, \quad \forall (x_t, x_{t+1}). \quad (41)$$

The right hand side does not depend on  $x_t$ , therefore, the left hand side is a constant. So we have

$$C_t(x_t) \propto \tilde{F}_t(x_t), \quad \forall t. \quad (42)$$

The probability of generating a data  $x_T$  then equals

$$P_F(x_T) = \int P_0(x_0|\odot) \prod_t P_F(x_{t+1}|x_t) dx_{0:T-1} \quad (43)$$

$$= \int P_0^\#(x_0|\odot) \prod_t P_F^\#(x_{t+1}|x_t) \prod_t \tilde{P}_F(x_{t+1}|x_t) dx_{0:T-1} \quad (44)$$

$$= \int P_0^\#(x_0|\odot) \prod_t P_F^\#(x_{t+1}|x_t) \frac{\tilde{F}_{t+1}(x_{t+1})}{C_t(x_t)} dx_{0:T-1} \quad (45)$$

$$\propto \tilde{F}_T(x_T) \int P_0^\#(x_0|\odot) \prod_t P_F^\#(x_{t+1}|x_t) dx_{0:T-1} \quad (46)$$

$$\propto R(x_T)^\beta P_F^\#(x_T). \quad (47)$$

This completes the validness proof.

#### B.4 RELATIONSHIP BETWEEN RESIDUAL DB AND TRAJECTORY BALANCE

Here we illustrate the Remark 5. A different but equivalent condition for GFlowNets states:

**Trajectory Balance (TB) [31].** The following TB condition must hold for any transition sequence  $(s_0, s_1, \dots, s_N)$  where  $x_0$  is the unique starting state in the MDP and  $s_N$  is a terminal state, given a GFlowNet with the forward policy  $P_F(s'|s)$  and the backward policy  $P_B(s|s')$ :

$$\log \frac{Z \prod P_F(s'|s)}{R(x_T) \prod P_B(s|s')} = 0 \quad (48)$$

where  $Z = F(x_0)$  is the total flow and  $R(x_T) = F(x_T)$  the reward. The proof is immediate with a telescoping product of the DB condition.

With an (ideal) pretrained model  $P_F^\#$  and the satisfaction of the finetuning objective of Equation 10, one can prove the conclusion in [55]:

$$\log \frac{Z \prod P_F(s'|s)}{Z^\# \prod P_F^\#(s'|s)} = \beta \log R(x_T), \quad (49)$$

which is also an immediate result of a telescoping products of the *residual* DB condition (which leads to Equation 20):

$$\log \tilde{P}_F(x_{t+1}|x_t) = \log \tilde{F}(x_{t+1}) - \log \tilde{F}(x_t). \quad (50)$$

While Equation 49 and residual DB are mathematically equivalent, implementation-wise TB in Equation 49 demands the whole sampling sequence be stored in the memory for gradient computation, or one has resort to the time-costly technique of gradient checkpointing. In comparison, with DB-based methods one may amortize the computational cost into flows at different time steps and therefore allow diffusion finetuning with flexible sampling sequence, of which the distribution approximation capacity and generation performance are generally greater.

## C CORRECTIONS FOR NON-IDEAL PRETRAINED MODELS

For non-ideal pretrained models in which  $P_F^\#$  does not match  $P_B$  (*i.e.*, the DB condition is violated), the original *residual*  $\nabla$ -DB objective is apparently biased. We may introduce an additional learnable term  $h(x_t, x_{t+1}; \psi)$  to compensate for this error, with which we obtain:

$$L_{\nabla\text{DB-res-v2}}(x_t, x_{t+1}) = \left\| \nabla_{x_{t+1}} \log \tilde{P}_F(x_{t+1}|x_t) - \nabla_{x_{t+1}} \log \tilde{F}(x_{t+1}) + \nabla_{x_{t+1}} h(x_t, x_{t+1}; \psi) \right\|^2 \quad (51)$$

and

$$L_{\nabla\text{DB-res-v2}}(x_t, x_{t+1}) = \left\| \nabla_{x_t} \log \tilde{P}_F(x_{t+1}|x_t) + \nabla_{x_t} \log \tilde{F}(x_{t+1}) + \nabla_{x_t} h(x_t, x_{t+1}; \psi) \right\|^2. \quad (52)$$

## D FINETUNING CONVERGENCE IN WALL TIME

We further show the convergence speed measured in relative wall time on a single node with 8 80GB-mem A100 GPUs in Fig. 9.

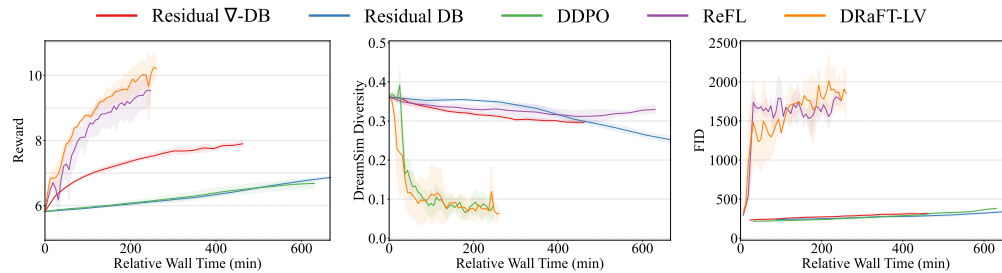


Figure 9: Convergence curves of different metrics for different methods throughout the finetuning process on Aesthetic Score, with the  $x$ -axis being the relative wall time. All methods are benchmarked on a single node with 8 80GB-mem A100 GPUs.



E FIGURES FOR ABLATION RESULTS

1080  
1081  
1082  
1083  
1084  
1085  
1086  
1087  
1088  
1089  
1090  
1091  
1092  
1093  
1094  
1095  
1096  
1097  
1098  
1099  
1100  
1101  
1102  
1103  
1104  
1105  
1106  
1107  
1108  
1109  
1110  
1111  
1112  
1113  
1114  
1115  
1116  
1117  
1118  
1119  
1120  
1121  
1122  
1123  
1124  
1125  
1126  
1127  
1128  
1129  
1130  
1131  
1132  
1133

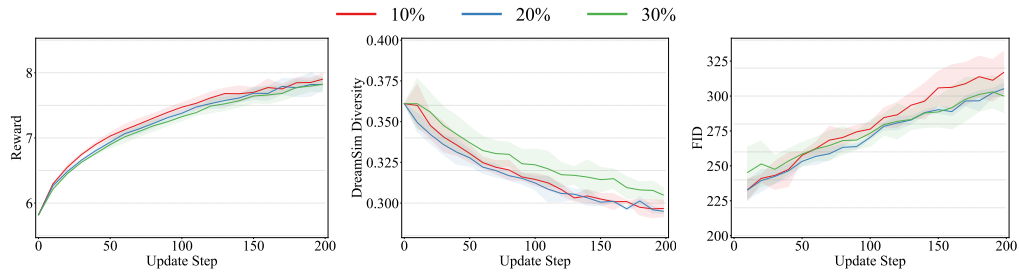


Figure 10: Ablation study on the effect of subsampling rate on the collected trajectories for computing the residual  $\nabla$ -DB loss.

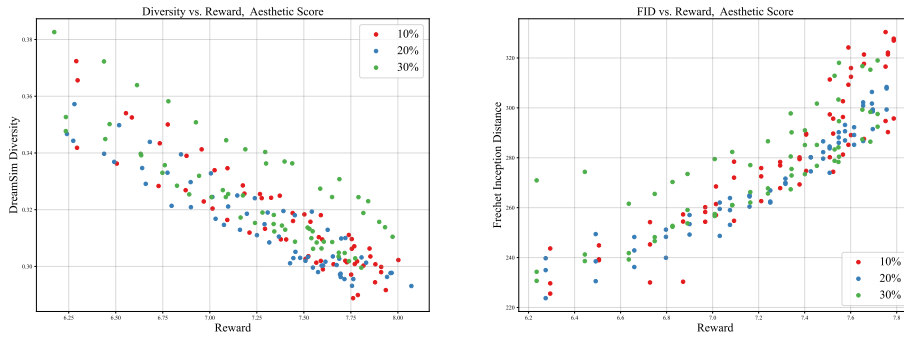


Figure 11: Pareto frontiers for reward, diversity and prior-following (measured by FID) of models trained with different subsampling rate. In expectation, higher subsampling rates seem to slightly help in increasing diversity.

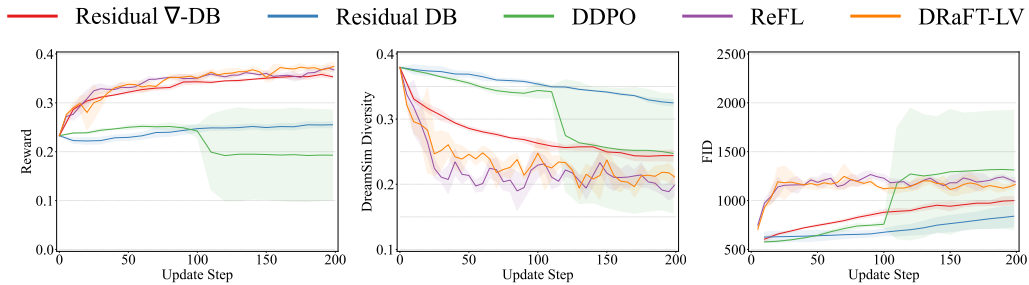


Figure 12: Convergence curve of metrics of different methods throughout the finetuning process on the HPSv2 reward model.

1134  
1135  
1136  
1137  
1138  
1139  
1140  
1141  
1142  
1143  
1144  
1145

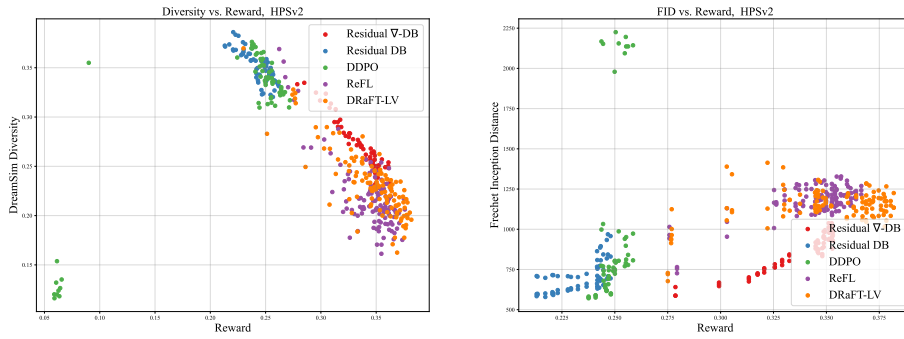


Figure 13: Pareto frontiers for reward, diversity and prior-following (measured by FID) on HPSv2.

1146  
1147  
1148  
1149  
1150  
1151  
1152  
1153  
1154  
1155  
1156  
1157  
1158

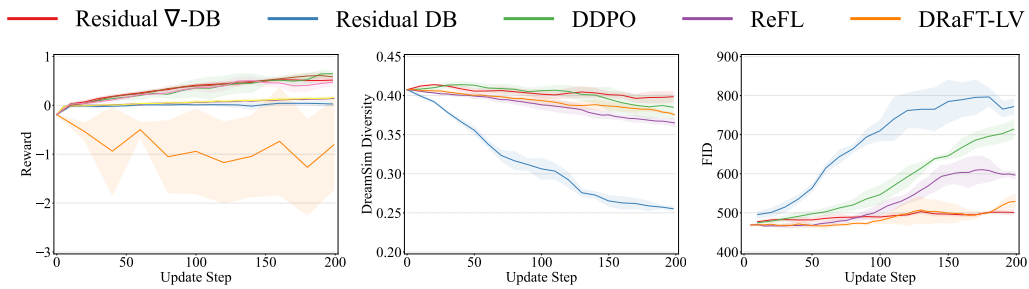


Figure 14: Convergence curve of metrics of different methods throughout the finetuning process on the ImageReward reward model.

1159  
1160  
1161  
1162  
1163  
1164  
1165  
1166  
1167  
1168  
1169  
1170  
1171  
1172  
1173

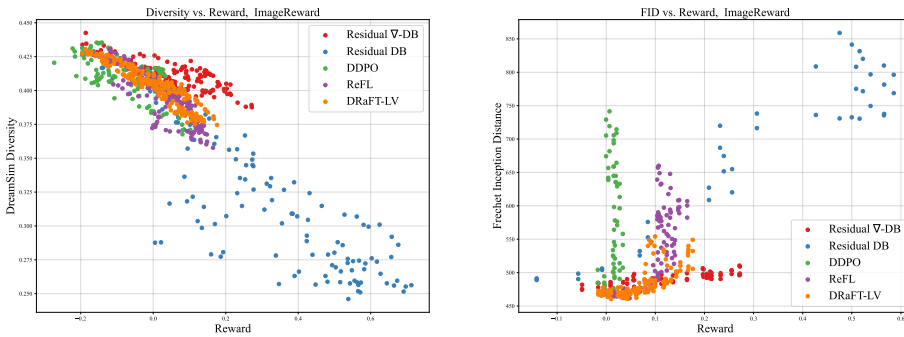


Figure 15: Pareto frontiers for reward, diversity and prior-following (measured by FID) on ImageReward.

1174  
1175  
1176  
1177  
1178  
1179  
1180  
1181  
1182  
1183  
1184  
1185  
1186  
1187

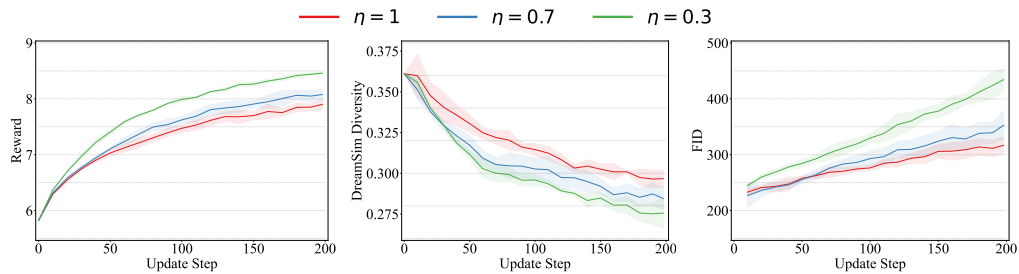


Figure 16: Convergence curve of metrics of different methods throughout the finetuning process on Aesthetic Score with different strength of prior  $\eta$ .

1188  
 1189  
 1190  
 1191  
 1192  
 1193  
 1194  
 1195  
 1196  
 1197  
 1198  
 1199  
 1200  
 1201  
 1202  
 1203  
 1204  
 1205  
 1206  
 1207  
 1208  
 1209  
 1210  
 1211  
 1212  
 1213  
 1214  
 1215  
 1216  
 1217  
 1218  
 1219  
 1220  
 1221  
 1222  
 1223  
 1224  
 1225  
 1226  
 1227  
 1228  
 1229  
 1230  
 1231  
 1232  
 1233  
 1234  
 1235  
 1236  
 1237  
 1238  
 1239  
 1240  
 1241

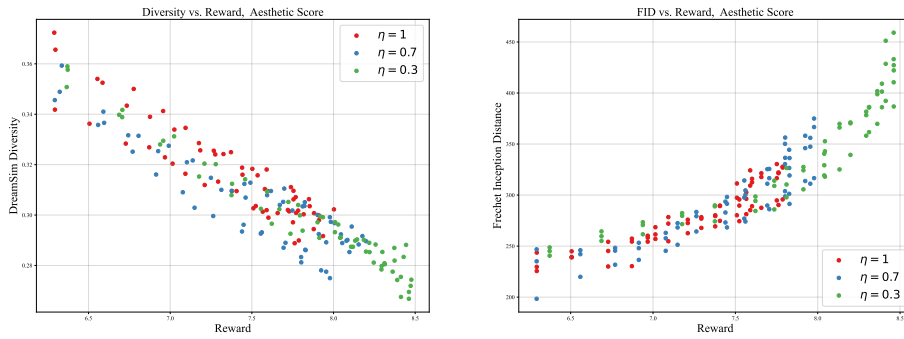


Figure 17: Pareto frontiers for reward, diversity and prior-following (measured by FID) on Aesthetic Score with different strength of prior  $\eta$ .

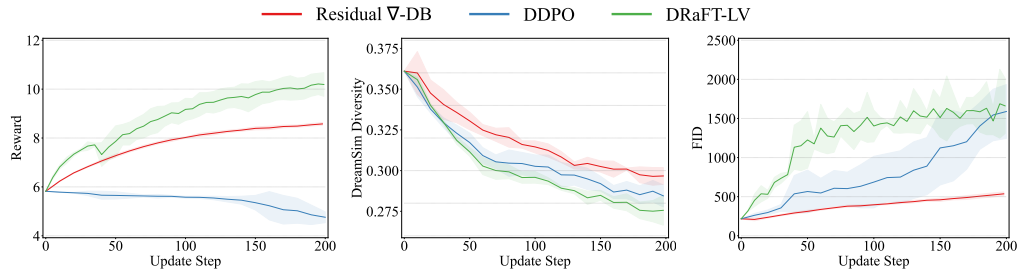


Figure 18: Convergence curve of metrics of different methods throughout the finetuning process on Aesthetic Score with the MDP constructed by SDE-DPM-Solver++ (with 20 inference steps).

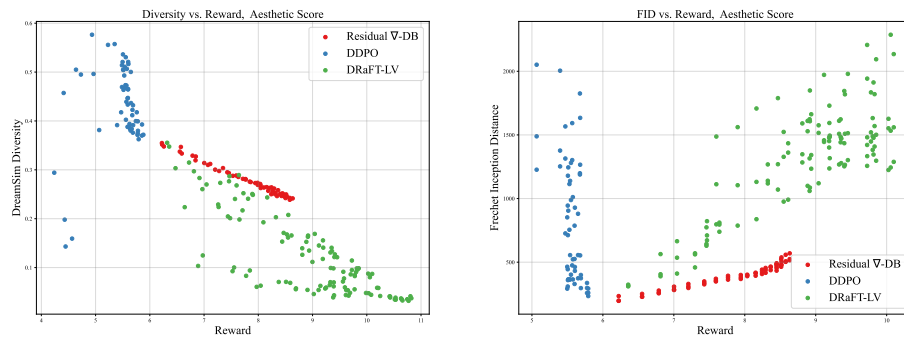


Figure 19: Pareto frontiers for reward, diversity and prior-following (measured by FID) on Aesthetic Score with the MDP constructed by SDE-DPM-Solver++ (with 20 inference steps).

## F ADDITIONAL ABLATION EXPERIMENTS

**Effect of attenuating scaling on predicted reward.** In Fig. 20 and 21, we show the comparison between models with and without time-dependent attenuation of reward signals, where both models are trained with  $\beta = 10000$ . While setting  $\gamma_t = 1$  for all  $t$  can slightly increase the convergence speed, it comes at the cost of worse diversity and prior-following capability.

**Effect of 2nd-order gradients in finetuning.** In Fig. 22 and 23, we show the comparison between models with and without 2nd-order gradients, where both models are trained with  $\beta = 10000$ . Empirically, 2nd-order gradients hurts the trade-off between reward convergence, diversity preservation and prior following.

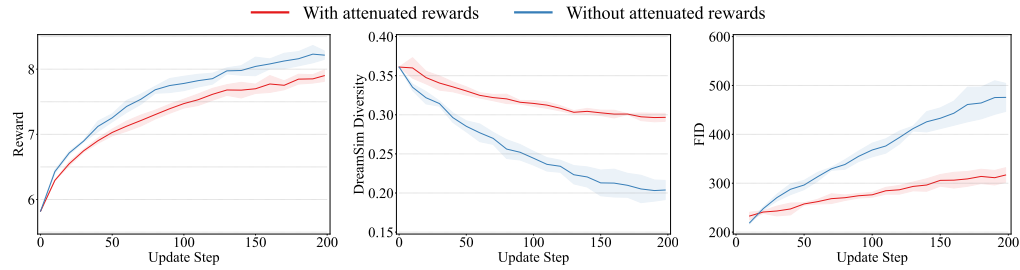


Figure 20: Convergence curve of metrics of different methods throughout the finetuning process on Aesthetic Score with time-dependent attenuation of predicted rewards. Both models are trained with  $\beta = 10000$ . With decayed predicted rewards, the convergence speed is slower but due to less aggressive prediction on reward signal, the model with reward attenuation achieves better diversity and prior-following results.

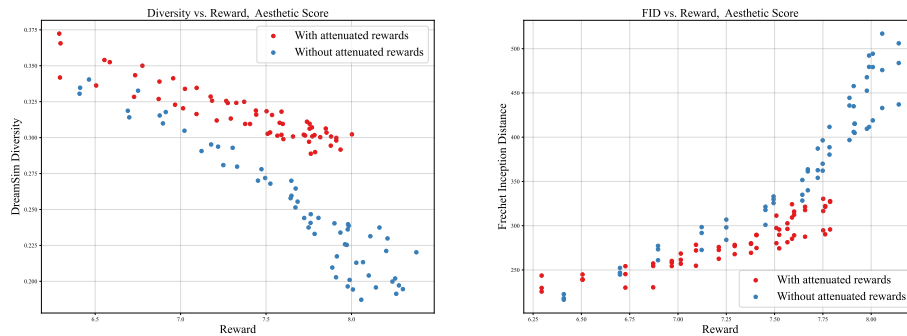


Figure 21: Pareto frontiers for reward, diversity and prior-following (measured by FID) on Aesthetic Score with time-dependent scaling of predicted rewards.

1296  
1297  
1298  
1299  
1300  
1301  
1302  
1303  
1304  
1305  
1306  
1307  
1308  
1309  
1310  
1311  
1312  
1313  
1314  
1315  
1316  
1317  
1318  
1319  
1320  
1321  
1322  
1323  
1324  
1325  
1326  
1327  
1328  
1329  
1330  
1331  
1332  
1333  
1334  
1335  
1336  
1337  
1338  
1339  
1340  
1341  
1342  
1343  
1344  
1345  
1346  
1347  
1348  
1349

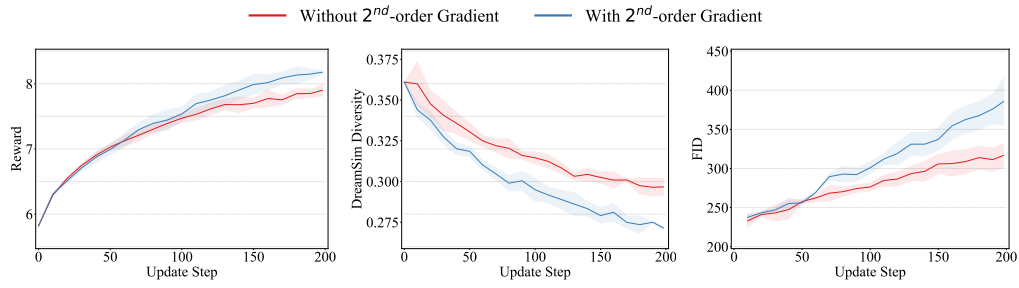


Figure 22: Convergence curve of metrics of different methods throughout the finetuning process on Aesthetic Score with and without 2nd-order gradients.

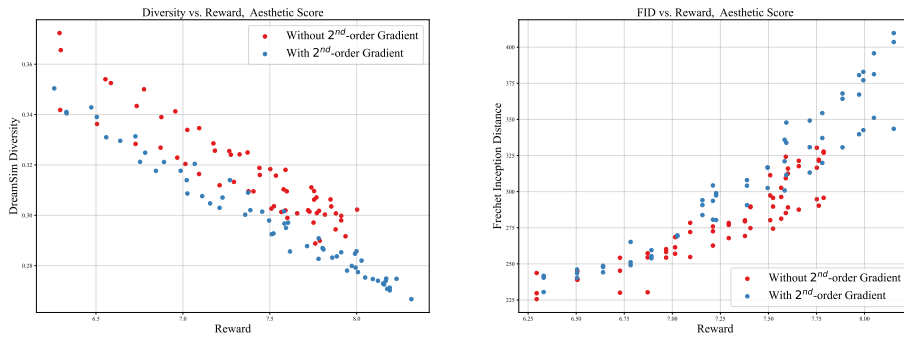


Figure 23: Pareto frontiers for reward, diversity and prior-following (measured by FID) on Aesthetic Score with and without 2nd-order gradients.

1350 G MORE SAMPLES (AESTHETIC SCORE)

1351  
1352  
1353  
1354  
1355  
1356  
1357  
1358  
1359  
1360  
1361  
1362  
1363  
1364  
1365  
1366  
1367  
1368  
1369  
1370  
1371  
1372  
1373  
1374  
1375  
1376  
1377  
1378  
1379  
1380  
1381  
1382  
1383  
1384  
1385  
1386  
1387  
1388  
1389  
1390  
1391  
1392  
1393  
1394  
1395  
1396  
1397  
1398  
1399  
1400  
1401  
1402  
1403



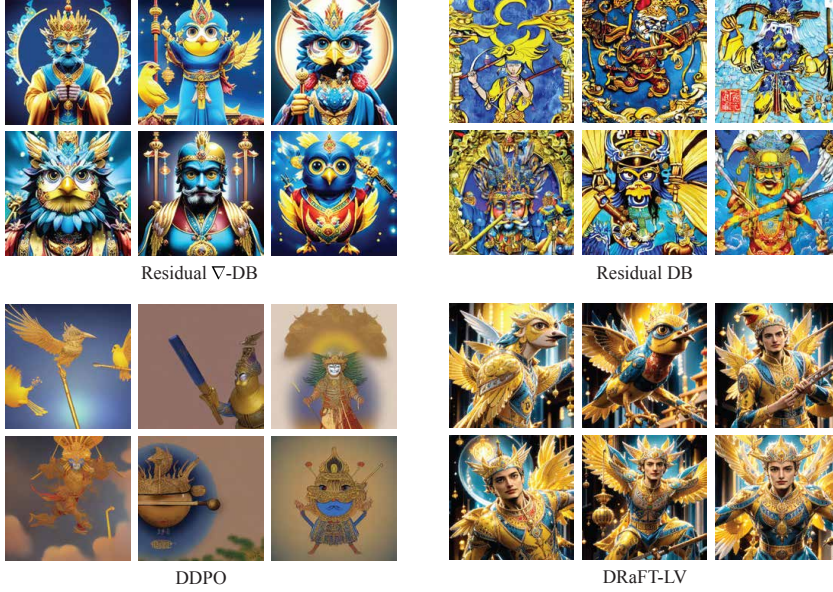
Figure 24: Additional uncensored samples from the model finetuned with *residual*  $\nabla$ -DB on the reward model of Aesthetic Score.



H MORE SAMPLES (HPSv2)

1404  
1405  
1406  
1407  
1408  
1409  
1410  
1411  
1412  
1413  
1414  
1415  
1416  
1417  
1418  
1419  
1420  
1421  
1422  
1423  
1424  
1425  
1426  
1427  
1428  
1429  
1430  
1431  
1432  
1433  
1434  
1435  
1436  
1437  
1438  
1439  
1440  
1441  
1442  
1443  
1444  
1445  
1446  
1447  
1448  
1449  
1450  
1451  
1452  
1453  
1454  
1455  
1456  
1457

Prompt: An ultra-realistic illustration of a **bird god** swinging a **gold metal stick** weapon, with a **blue man face** and yellow bird mouth, and intricate traditional Chinese elements..



Prompt: A female **archer elf** leads a group of adventurers through a forest of crystal trees in a fantasy matte painting.

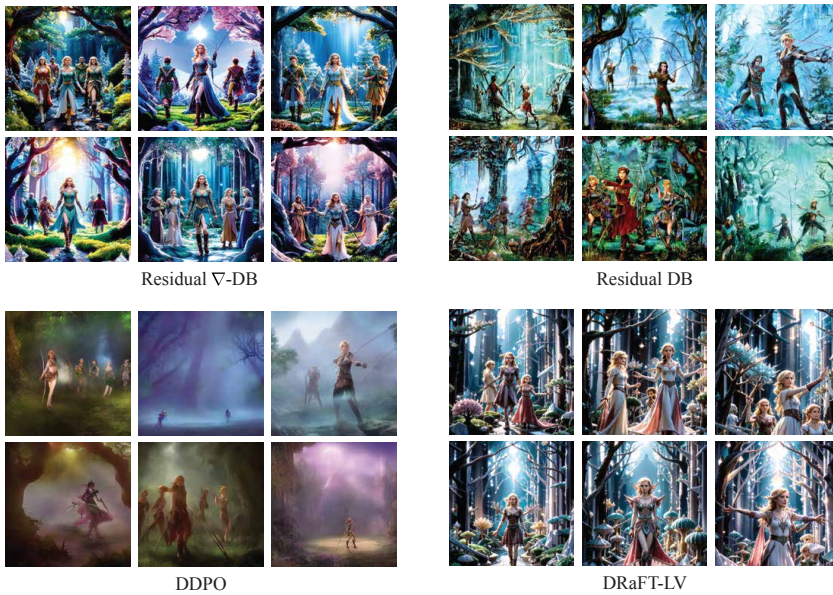


Figure 25: More comparison between samples generated by *residual*  $\nabla$ -DB and the baseline methods. The model finetuned with *residual*  $\nabla$ -DB is capable of following the instructions while generating diverse samples.

1458  
1459  
1460  
1461  
1462  
1463  
1464  
1465  
1466  
1467  
1468  
1469  
1470  
1471  
1472  
1473  
1474  
1475  
1476  
1477  
1478  
1479  
1480  
1481  
1482  
1483  
1484  
1485  
1486  
1487  
1488  
1489  
1490  
1491  
1492  
1493  
1494  
1495  
1496  
1497  
1498  
1499  
1500  
1501  
1502  
1503  
1504  
1505  
1506  
1507  
1508  
1509  
1510  
1511

Prompt: A surreal cat with a smile and intricate details.



Prompt: Redhead punk girl playing electric guitar in an oil painting masterpiece.

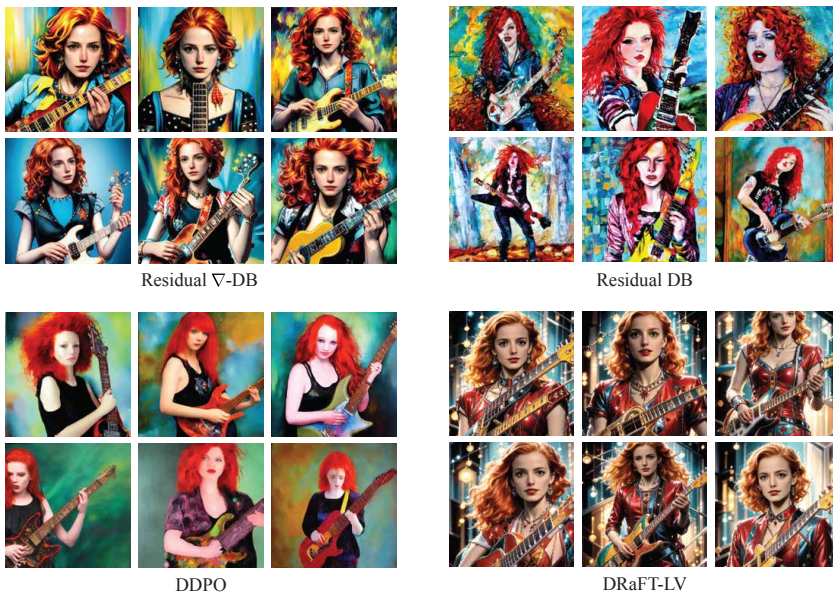


Figure 26: HPSv2 samples, Continued.